

Extended theoretical transition data in C I–IV

W. Li,^{1,3}^{*} A. M. Amarsi,² A. Papoulia^{1,3} J. Ekman¹ and P. Jönsson¹

¹Department of Materials Science and Applied Mathematics, Malmö University, SE-205 06, Malmö, Sweden

²Theoretical Astrophysics, Department of Physics and Astronomy, Uppsala University, Box 516, SE-751 20 Uppsala, Sweden

³Division of Mathematical Physics, Lund University, Post Office Box 118, SE-221 00 Lund, Sweden

Accepted XXX. Received YYY; in original form ZZZ

ABSTRACT

Accurate atomic data are essential for opacity calculations and for abundance analyses of the Sun and other stars. The aim of this work is to provide accurate and extensive results of energy levels and transition data for C I–IV.

The Multiconfiguration Dirac–Hartree–Fock and relativistic configuration interaction methods were used in the present work. To improve the quality of the wave functions and reduce the relative differences between length and velocity forms for transition data involving high Rydberg states, alternative computational strategies were employed by imposing restrictions on the electron substitutions when constructing the orbital basis for each atom and ion.

Transition data, e.g., weighted oscillator strengths and transition probabilities, are given for radiative electric dipole (E1) transitions involving levels up to $1s^22s^22p6s$ for C I, up to $1s^22s^27f$ for C II, up to $1s^22s7f$ for C III, and up to $1s^28g$ for C IV. Using the difference between the transition rates in length and velocity gauges as an internal validation, the average uncertainties of all presented E1 transitions are estimated to be 8.05%, 7.20%, 1.77%, and 0.28%, respectively, for C I–IV. Extensive comparisons with available experimental and theoretical results are performed and good agreement is observed for most of the transitions. In addition, the C I data were employed in a reanalysis of the solar carbon abundance. The new transition data give a line-by-line dispersion similar to the one obtained when using transition data that are typically used in stellar spectroscopic applications today.

Key words: Atomic data — Atomic processes — Line: formation — Radiative transfer — Sun: abundances — Methods: numerical

1 INTRODUCTION

Accurate atomic data are of fundamental importance to many different fields of astronomy and astrophysics. This is particularly true for carbon. As the fourth-most abundant metal in the cosmos (Asplund et al. 2009), carbon is a major source of opacity in the atmospheres and interiors of stars. Complete and reliable sets of atomic data for carbon are essential for stellar opacity calculations, because of their significant impact on stellar structure and evolution (e.g. Vandenberg et al. 2012; Chen et al. 2020).

Accurate atomic data for carbon are also important in the context of spectroscopic abundance analyses and Galactic Archaeology. Carbon abundances measured in late-type stars help us to understand the nucleosynthesis of massive stars and AGB stars, and thus the Galactic chemical evolution (e.g. Franchini et al. 2020; Jofré et al. 2020; Stonkutė et al. 2020). In early-type stars, carbon abundances help constrain the present-day Cosmic Abundance Standard (e.g. Nieva & Przybilla 2008, 2012; Alexeeva et al. 2019). In the Sun, the carbon abundance is precisely measured in order to put different cosmic objects onto a common scale (e.g. Caffau et al. 2010; Amarsi et al. 2019). In all of these cases, oscillator strengths for C I (cool stars) and for C I–IV (hot stars) underpin the spectroscopic analyses; this is especially the case for studies that relax the assumption of local

thermodynamic equilibrium (LTE; e.g. Przybilla et al. 2001; Nieva & Przybilla 2006), in which case much larger sets of reliable atomic data are needed.

On the experimental side, a number of studies of transition data have been presented in the literature. Neutral C I transition probabilities for the $2p4p \rightarrow 2p3s$ transition array have been studied by Miller et al. (1974) using a spectroscopic shock tube and by Jones & Wiese (1984) using a wall-stabilized arc. The measurements of relative oscillator strengths for $2p3p \rightarrow 2p3s$, $2p3d \rightarrow 2p3p$ and $2p4s \rightarrow 2p3p$ have been performed by Musielok et al. (1997); Bacawski et al. (2001); Golly et al. (2003) using a wall-stabilized arc. Older measurements of oscillator strengths are also available using the same technique (Maecker 1953; Richter 1958; Foster 1962; Boldt 1963; Goldbach & Nollez 1987; Goldbach et al. 1989). By analysing the high-resolution spectra obtained with the Goddard High Resolution Spectrograph on the Hubble Space Telescope, Federman & Zsargo (2001) derived oscillator strengths for C I lines below 1200 Å.

For C II, a number of measurements have also been performed. Träbert et al. (1999) measured the radiative decay rates for the intercombination (IC) transitions $2s2p^2\ ^4P \rightarrow 2s^22p\ ^2P^o$ at a heavy-ion storage ring, and the total measured radiative decay rates to the ground term were $125.8 \pm 0.9\text{ s}^{-1}$ for $^4P_{1/2}$, $9.61 \pm 0.05\text{ s}^{-1}$ for $^4P_{3/2}$, and $45.35 \pm 0.15\text{ s}^{-1}$ for $^4P_{5/2}$. The aforementioned results are, however, not in agreement with the values measured by Fang et al. (1993) using a radio-frequency ion trap, i.e., $146.4(+8.3, -9.2)\text{ s}^{-1}$ for $^4P_{1/2}$,

^{*} E-mail: wenxian.li@mau.se

11.6(+0.8, -1.7) s⁻¹ for 4P_{3/2}, and 51.2(+2.6, -3.5) s⁻¹ for 4P_{5/2}. Goly & Weniger (1982) measured the transition probabilities for a helium-carbon arc for some multiplets of {2p³, 2s²3p} → 2s2p² and 2s²4s → 2s²3p with estimated relative uncertainty of 50%. Using an electric shock tube, Roberts & Eckerle (1967) provided the relative oscillator strengths of some C II multiplets with relative uncertainties of 7%. Reistad et al. (1986) gave lifetimes for 11 C II levels using the beam-foil excitation technique and extensive cascade analyses.

For C III, the IC decay rate of the 2s2p ³P₁^o → 2s² ¹S₀ transition was measured to be 121.0 ± 7 s⁻¹ by Kwong et al. (1993) using a radio-frequency ion trap and 102.94 ± 0.14 s⁻¹ by Doerfert et al. (1997) using a heavy-ion storage ring. The discrepancy between the values obtained from the two different methods is quite large, i.e., of the order of 15%. The result given by the latter measurement is closer to earlier *ab initio* calculations ranging between 100 and 104 s⁻¹ (Fleming et al. 1994; Fischer 1994; Ynnerman & Fischer 1995). Several measurements have also been performed for the lifetimes of the low-lying levels of C III (Reistad & Martinson 1986; Mickey 1970; Nandi et al. 1996; Buchet-Poulizac & Buchet 1973a).

For the system of Li-like C IV, the transition probabilities of the 1s²2p ²P_{1/2,3/2}^o → 1s²2s ²S_{1/2} transitions were measured by Berkner et al. (1965) using the foil-excitation technique and by Knystautas et al. (1971) using the beam-foil technique, respectively. There are also a number of measurements of lifetimes in C IV using the beam-foil technique (Donnelly et al. 1978; Buchet-Poulizac & Buchet 1973b; Jacques et al. 1980).

On the theoretical side, Froese Fischer et al. have performed detailed studies of C I–IV, focusing on the low-lying levels. They carried out Multiconfiguration Hartree-Fock (MCHF) calculations and used the Breit-Pauli (MCHF-BP) approximation for computing energy levels and transition properties, e.g., transition probabilities, oscillator strengths, and lifetimes, in C I (Tachiev & Fischer 2001; Fischer 2006; Fischer & Tachiev 2004), C II (Tachiev & Fischer 2000), C III (Tachiev & Fischer 1999; Fischer 2000), and C IV (Godefroid et al. 2001; Fischer et al. 1998).

Hibbert et al. have presented extensive calculations for optical transitions. They used the CIV3 code (Hibbert 1975) to calculate oscillator strengths and transition probabilities in C I (Hibbert et al. 1993), C II (Corrége & Hibbert 2004), and C III (Kingston & Hibbert 2000). In the calculations of Hibbert et al. (1993); Corrége & Hibbert (2004), empirical adjustments were introduced to the diagonal matrix elements in order to accurately reproduce energy splittings. Their C I oscillator strengths are frequently used in the abundance analyses of cool stars (Sect. 5).

A number of other authors have also presented theoretical transition data for carbon. Zatsarinny & Fischer (2002) calculated the oscillator strengths for transitions to high-lying excited states of C I using a spline frozen-cores method. Nussbaumer & Storey (1984) provided the radiative transition probabilities using the *LS*-coupling approximation and intermediate coupling approximation, respectively, for the six energetically lowest configurations of C I. Nussbaumer & Storey (1981) calculated the transition probabilities for C II, from terms up to 2s²4f ²F^o, using the *LS*-coupling and close coupling (CC) approximation, respectively.

In view of the great astrophysical interest for large sets of homogeneous atomic data, extensive spectrum calculations of transition data in the carbon atom and carbon ions were carried out under the umbrella of the Opacity Project using the CC approximation of the R-matrix theory, and the results are available in the Opacity Project online database (TOPbase; Cunto & Mendoza (1992); Cunto et al. (1993)). The latest compilation of C I transition probabilities was

made available by Haris & Kramida (2017), and those of C II–IV can be found in earlier compilations by Wiese & Fuhr (2007b,a) and Fuhr (2006).

In this context, the General-purpose Relativistic Atomic Structure Package (GRASP) has, more recently, been used by Aggarwal & Keenan (2015) to predict the radiative decay rates and lifetimes of 166 levels belonging to the n ≤ 5 configurations in C III. Using an updated and extended version of this code (GRASP2K), Jönsson et al. (2010) determined transition data involving 26 levels in C II.

Although for the past decades a considerable amount of research has been conducted for carbon, there is still a need for extended sets of reliable theoretical transition data. To address this, we have carried out new calculations based on the fully relativistic Multiconfiguration Dirac–Hartree–Fock (MCDHF) and relativistic configuration interaction (RCI) methods, as implemented in the newest version of the GRASP code, GRASP2018 (Jönsson et al. 2013; Fischer et al. 2019). We performed energy spectrum calculations for 100, 69, 114, and 53 states, in C I–IV, respectively. Electric dipole (E1) transition data (wavelengths, transition probabilities, line strengths, and oscillator strengths) were computed along with the corresponding lifetimes of these states.

This paper is structured into six sections, including the introduction. Our theoretical methods are described in Sect. 2, and computational details are given in Sect. 3. In Sect. 4, we present our results and the validation of the data. As a complementary method of validation, in Sect. 5, we use the derived data in a reanalysis of the solar carbon abundance. Finally, we present our conclusions in Sect. 6.

2 THEORY

In the Multiconfiguration Dirac–Hartree–Fock (MCDHF) method (Grant 2007; Fischer et al. 2016), wave functions for atomic states $\gamma^{(j)} P J M$, $j = 1, 2, \dots, N$ with angular momentum quantum numbers $J M$ and parity P are expanded over N_{CSFs} configuration state functions

$$\Psi(\gamma^{(j)} P J M) = \sum_i^{N_{\text{CSFs}}} c_i^{(j)} \Phi(\gamma_i P J M). \quad (1)$$

The configuration state functions (CSFs) are *jj*-coupled many-electron functions, recursively built from products of one-electron Dirac orbitals. As for the notation, γ_i specifies the occupied subshells of the CSF with their complete angular coupling tree information. The radial large and small components of the one-electron orbitals and the expansion coefficients $\{c_i^{(j)}\}$ of the CSFs are obtained, for a number of targeted states, by solving the Dirac–Hartree–Fock radial equations and the configuration interaction eigenvalue problem resulting from applying the variational principle on the statistically weighted energy functional of the targeted states with terms added for preserving the orthonormality of the one-electron orbitals. The energy functional is based on the Dirac–Coulomb (DC) Hamiltonian and accounts for relativistic kinematic effects.

Once the radial components of the one-electron orbitals are determined, higher-order interactions, such as the transverse photon interaction and quantum electrodynamic (QED) effects (vacuum polarization and self-energy), are added to the Dirac–Coulomb Hamiltonian. Keeping the radial components fixed, the expansion coefficients $\{c_i^{(j)}\}$ of the CSFs for the targeted states are obtained by solving the configuration interaction eigenvalue problem.

The evaluation of radiative E1 transition data (transition probabilities, oscillator strengths) between two states: $\gamma' P' J' M'$ and $\gamma P J M$ is

non-trivial. The transition data can be expressed in terms of reduced matrix elements of the transition operator $\mathbf{T}^{(1)}$:

$$\langle \Psi(\gamma PJ) \| \mathbf{T}^{(1)} \| \Psi(\gamma' P' J') \rangle = \sum_{j,k} c_j c'_k \langle \Phi(\gamma_j PJ) \| \mathbf{T}^{(1)} \| \Phi(\gamma'_k P' J') \rangle, \quad (2)$$

where c_j and c'_k are, respectively, the expansion coefficients of the CSFs for the lower and upper states, and the summation occurs over all the CSFs for the lower and upper states. The reduced matrix elements are expressed via spin-angular coefficients $d_{ab}^{(1)}$ and operator strengths as:

$$\langle \Phi(\gamma_j PJ) \| \mathbf{T}^{(1)} \| \Phi(\gamma'_k P' J') \rangle = \sum_{a,b} d_{ab}^{(1)} \langle n_a l_a j_a \| \mathbf{T}^{(1)} \| n_b l_b j_b \rangle. \quad (3)$$

Allowing for the fact that we are now using Brink-and-Satchler type reduced matrix elements, we have

$$\langle n_a l_a j_a \| \mathbf{T}^{(1)} \| n_b l_b j_b \rangle = \left(\frac{(2j_b + 1)\omega}{\pi c} \right)^{1/2} (-1)^{j_a - 1/2} \begin{pmatrix} j_a & 1 & j_b \\ \frac{1}{2} & 0 & -\frac{1}{2} \end{pmatrix} \overline{M}_{ab}, \quad (4)$$

where \overline{M}_{ab} is the radiative transition integral defined by Grant (1974). The factor in front of \overline{M}_{ab} is the Wigner 3-j symbol that gives the angular part of the matrix element. The \overline{M}_{ab} integral can be written $\overline{M}_{ab} = \overline{M}_{ab}^e + G \overline{M}_{ab}^l$, where G is the gauge parameter. When $G = 0$ we get the Coulomb gauge, whereas for $G = \sqrt{2}$ we get the Babushkin gauge. The Babushkin gauge corresponds to the length gauge in the non-relativistic limit and puts weight on the outer part of the wave functions (Grant 1974; Hibbert 1974). The Coulomb gauge corresponds to the velocity gauge and puts more weight on the inner part of the wave functions (Papoulia et al. 2019). For E1 transitions, the Babushkin and Coulomb gauges give the same value of the transition moment for exact solutions of the Dirac-equation (Grant 1974). For approximate solutions, the transition moments differ, and the quantity dT , defined as (Froese Fischer 2009; Ekman et al. 2014)

$$dT = \frac{|A_l - A_v|}{\max(A_l, A_v)}, \quad (5)$$

where A_l and A_v are transition rates in length and velocity form, can be used as an estimation of the uncertainty of the computed rate.

3 COMPUTATIONAL SCHEMES

Calculations were performed in the extended optimal level (EOL) scheme (Dyall et al. 1989) for the weighted average of the even and odd parity states. The CSF expansions were determined using the multireference-single-double (MR-SD) method, allowing single and double (SD) substitutions from a set of important configurations, referred to as the MR, to orbitals in an active set (AS) (Olsen et al. 1988; Sturesson et al. 2007; Fischer et al. 2016). The orbitals in the AS are divided into spectroscopic orbitals, which build the configurations in the MR, and correlation orbitals, which are introduced to correct the initially obtained wave functions. During the different steps of the calculations for C I–IV, the CSF expansions were systematically enlarged by adding layers of correlation orbitals.

MCDHF calculations aim to generate an orbital set. The orbital set is then used in RCI calculations based on CSF expansions that can be enlarged to capture additional electron correlation effects. For

the same CSF expansion, different orbital sets give different results for both energy levels and transition data. Conventionally, MCDHF calculations are performed for CSF expansions obtained by allowing substitutions not only from the valence subshells, but also from the subshells deeper in the core, accounting for valence-valence (VV), core-valence (CV), and core-core (CC) electron correlation effects. Using orbital sets from such calculations, Pehlivan Rhodin et al. (2017) predicted large dT values for transitions between low-lying states and high Rydberg states, indicating substantial uncertainties in the corresponding transition data. For transitions involving high Rydberg states, it was shown that the velocity gauge gave the more accurate results, which is contradictory to the general belief that the length gauge is the preferred one (Hibbert 1974). Analyzing the situation more carefully, Papoulia et al. (2019) found that correlation orbitals resulting from MCDHF calculations based on CSF expansions obtained by allowing substitutions from deeper subshells are very contracted in comparison with the outer Rydberg orbitals. As a consequence, the outer parts of the wave functions for the Rydberg states are not accurately described. Thus, the length form that probes the outer part of the wave functions does not produce trustworthy results, while the velocity form that probes the inner part of the wave functions yields more reliable transition rates. In the same work, the authors showed how transition rates that are only weakly sensitive to the choice of gauge can be obtained, by paying close attention to the CSF generation strategies for the MCDHF calculations.

In the present work, following the suggestion by Papoulia et al. (2019), the MCDHF calculations were based on CSF expansions for which we impose restrictions on the substitutions from the inner subshells and obtain, as a consequence, correlation orbitals that overlap more with the spectroscopic orbitals of the higher Rydberg states, adding to a better representation of the outer parts of the corresponding wave functions. The MR and orbital sets for each atom and ion are presented in Table 1. The computational scheme, including CSF generation strategies, for each atom and ion is discussed in detail below. The MCDHF calculations were followed by RCI calculations, including the Breit interaction and leading QED effects.

3.1 C I

As seen in Table 1, in the computations of neutral carbon, configurations with $n = 7$ ($l = s$); 6 ($l = p, d$), which are not of direct relevance, were included in the MR set to obtain orbitals that are spatially extended, improving the quality of the outer parts of the wave functions of the higher Rydberg states. The MCDHF calculations were performed using CSF expansions that were produced by SD substitutions from the valence orbitals of the configurations in the MR to the active set of orbitals, with the restriction of allowing maximum one substitution from orbitals with $n = 2$. The $1s^2$ core was kept closed and, at this point, the expansions of the atomic states accounted for VV electron correlation. As a final step, an RCI calculation was performed for the largest SD valence expansion augmented by a CV expansion. The CV expansion was obtained by allowing SD substitutions from the valence orbitals and the $1s^2$ core of the configurations in the MR, with the restriction that there should be at most one substitution from $1s^2$. The numbers of CSFs in the final even and odd state expansions are, respectively, 14 941 842 and 15 572 953, distributed over the different J symmetries.

3.2 C II

Similarly to the computations in C I, in the computations of the singly-ionized carbon, the configurations $2s^2 \{8s, 8p, 9s, 9p\}$, which are not

Table 1. Summary of the computational schemes for C I–IV. The first column displays the configurations of the targeted states. MR and AS, respectively, denote the multireference sets and the active sets of orbitals used in the MCDHF and RCI calculations, and N_{CSFs} are the numbers of generated CSFs in the final RCI calculations, for the even (e) and the odd (o) parity states.

Targeted configurations	MR	AS	N_{CSFs}
C I, $N_{\text{levels}} = 100$			
$2s2p^3$	$2s2p^3$	$\{11s, 10p, 10d, 9f, 7g, 6h\}$	e: 14 941 842
$2s^22p\{n_1s, n_2p, n_3d, 4f\}$	$2s^22p\{n_1s, n_2p, n_3d, 4f\}$		o: 15 572 953
$(3 \leq n_1 \leq 6, 2 \leq n_2 \leq 5, 3 \leq n_3 \leq 5)$	$(3 \leq n_1 \leq 6, 2 \leq n_2 \leq 6, 3 \leq n_3 \leq 5)$		
	$2p^3\{n_1s, n_2p, n_3d\}$		
	$(3 \leq n_1 \leq 6, 3 \leq n_2 \leq 5, 3 \leq n_3 \leq 6)$		
	$2s2p^2\{3s, 3p, 4p, 6p, 6d, 7s\}$		
	$2s2p\{n_1s, n_2p, n_3d, 4f\}6d$		
	$(3 \leq n_1 \leq 6, 3 \leq n_2 \leq 5, 3 \leq n_3 \leq 5)$		
C II, $N_{\text{levels}} = 69$			
$2s^2nl(n \leq 6, l \leq 4)$	$2s2p^2, 2s^2\{n_1s, n_2p, n_3d, n_4f, n_5g\}$	$\{14s, 14p, 12d, 12f, 10g, 8h\}$	e: 6 415 798
$2s^27l(l \leq 3)$	$(3 \leq n_1 \leq 9, 2 \leq n_2 \leq 9, 3 \leq n_3 \leq 7, 4 \leq n_4 \leq 7, 5 \leq n_5 \leq 6)$		o: 4 988 973
$2s2p^2, 2p^3,$	$2p^3, 2p^2\{n_1s, n_2p, n_3d, n_4f, n_5g\}$		
$2s2p3s, 2s2p3p$	$(3 \leq n_1 \leq 9, 4 \leq n_2 \leq 9, 3 \leq n_3 \leq 7, 4 \leq n_4 \leq 7, 5 \leq n_5 \leq 6)$		
	$2s2p3s, 2s2p3p$		
C III, $N_{\text{levels}} = 114$			
$2s^2nl(n \leq 7, l \leq 4)$	$2s^2nl(n \leq 7, l \leq 4)$	$\{12s, 12p, 12d, 12f, 11g, 8h\}$	e: 1 578 620
$2p^2, 2p\{3s, 3p, 3d\}$	$2p^2, 2p\{3s, 3p, 3d\}$		o: 1 274 147
C IV, $N_{\text{levels}} = 53$			
$1s^2nl(n \leq 8, l \leq 4)$	$1s^2nl(n \leq 8, l \leq 4)$	$\{14s, 14p, 14d, 12f, 12g, 8h, 7i\}$	e: 1 077 872
$1s^26h$	$1s^26h$		o: 1 287 706

our prime targets, were included in the MR set (see also Table 1). In this manner, we generated orbitals that are localized farther from the atomic core. The MCDHF calculations were performed using CSF expansions obtained by allowing SD substitutions from the valence orbitals of the MR configurations. During this stage, the $1s^2$ core remained frozen and the CSF expansions accounted for VV correlation. The final wave functions of the targeted states were determined in an RCI calculation, which included CSF expansions that were formed by allowing SD substitution from all subshells of the MR configurations, with the restriction that there should be at most one substitution from the $1s^2$ core. The numbers of CSFs in the final even and odd state expansions are, respectively, 6 415 798 and 4 988 973, distributed over the different J symmetries.

3.3 C III

In the computations of beryllium-like carbon, the MR simply consisted of the targeted configurations (see also Table 1). The CSF expansions used in the MCDHF calculations were obtained by allowing SD substitutions from the valence orbitals, accounting for VV correlation effects. The final wave functions of the targeted states were determined in subsequent RCI calculations, which included CSFs that were formed by allowing single, double, and triple (SDT) substitutions from all orbitals of the MR configurations, with the limitation of leaving no more than one hole in the $1s^2$ atomic core. The final even and odd state expansions, respectively, contained 1 578 620 and 1 274 147 CSFs, distributed over the different J symmetries.

3.4 C IV

Likewise the computations in C III, the MR in the computations of lithium-like carbon was solely represented by the targeted configurations (see also Table 1). In the MCDHF calculations, the CSF expansions were acquired by implementing SD electron substitutions from the configurations in the MR, with the restriction of allowing maximum one hole in the $1s^2$ core. In this case, the shape of the correlation orbitals was established by CSFs accounting for valence (V) and CV correlation effects. In the subsequent RCI calculations, the CSF expansions were enlarged by enabling all SDT substitutions from the orbitals in the MR to the active set of orbitals. The final expansions of the atomic states gave rise to 1 077 872 CSFs with even parity and 1 287 706 CSFs with odd parity, respectively, shared among the different J symmetry blocks.

4 RESULTS

The energy spectra and wave function composition in LS -coupling for the 100, 69, 114, and 53 lowest states, respectively, for C I–IV are given in Table A1. In the tables, the states are given with unique labels (Gaigalas et al. 2017), and the labelling is determined by the CSFs with the largest coefficient in the expansion of Eq. (1). We first summarise the results here, before discussing the individual ions in detail in Sects. 4.1–4.4, below.

The accuracy of the wave functions from the present calculations was evaluated by comparing the calculated energy levels with experimental data provided via the National Institute of Standards and Technology (NIST) Atomic Spectra Database (Kramida et al. 2019). In the left panel of Fig. 1, energy levels computed in this work are

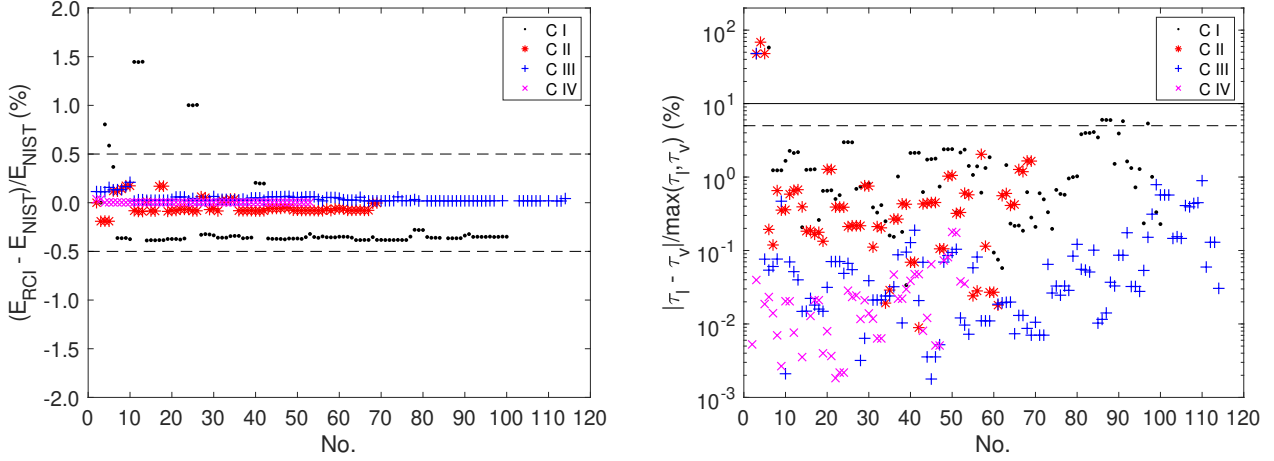


Figure 1. Left panel: Comparison of computed energy levels in the present work with data from the NIST database, for C I–IV. The dashed lines indicate the -0.5% and 0.5% relative discrepancies. Right panel: The relative differences between the lifetimes in length and velocity forms, for C I–IV. The dashed and solid lines indicate the 5% and 10% relative differences, respectively. No., as label in the x-axis, corresponds to the No. in Table A1.

compared with the NIST data. A closer inspection of the figure reveals that the relative discrepancies between the experimental and the computed in this work energies are, in most cases, about -0.35% , -0.08% , 0.03% , and 0.003% , respectively, for C I–IV. Only for levels of the $2s2p^3$ configuration in C I, the disagreements are larger than 1.0% . The average difference of the computed energy levels relative to the energies from the NIST database is 0.41% , 0.081% , 0.041% , and 0.0044% , respectively, for C I–IV. In Table A1, lifetimes in length and velocity gauges are also presented. The right panel of Fig. 1 presents the relative differences between the lifetimes in length and velocity forms for C I–IV. Except for a few long-lived states that can decay to the ground state only through IC transitions, the relative differences are well below 5%.

The accuracy of calculated transition rates can be estimated either by comparisons with other theoretical works and experimental results, when available, or by the quantity dT , which is defined in Eq. (5) as the agreement between the values in length and velocity gauges (Froese Fischer 2009; Ekman et al. 2014). The latter is particularly useful when no experimental measurements are available. Transition data, e.g., wavenumbers; wavelengths; line strengths; weighted oscillator strengths; transition probabilities of E1 transitions; and the accuracy indicators dT , are given in Tables A2 – A5, respectively, for C I–IV. Note that, the wavenumbers and wavelengths are adjusted to match the level energy values in the NIST database, which are critically evaluated by Haris & Kramida (2017) for C I and Moore & Gallagher (1993) for C II–IV. When no NIST values are available, the wavenumbers and wavelengths are from the present MCDHF/RCI calculations and marked with * in the tables.

To better display the uncertainties dT of the computed transitions rates and their distribution in relation to the magnitude of the transition rate values A , the transitions are organized in five groups based on the magnitude of the A values. A statistical analysis of the uncertainties dT of the transitions is performed for the 1553, 806, 1805, and 386 E1 transitions, respectively, for C I–IV. In Table 2, the mean value of the uncertainties $\langle dT \rangle$ and standard deviations σ are given for each group of transitions. As seen in Table 2, most of the estimated uncertainties dT are well below 10%. Most of the strong transitions with $A > 10^6 \text{ s}^{-1}$ are associated with small uncertainties dT , less than 2%, especially for C III and C IV, for which $\langle dT \rangle$ is 0.297% ($\sigma = 0.01$) and 0.205% ($\sigma = 0.0041$), respectively. It is worth noting that,

by employing the alternative optimization scheme of the radial orbitals in the present calculations, the uncertainties dT for transitions involving high Rydberg states are significantly reduced.

Contrary to the strong transitions, the weaker transitions are associated with relatively large dT values. This is even more pronounced for the first two groups of transitions in C I and C II, where A is less than 10^2 s^{-1} . These weak E1 transitions are either IC or two-electron one-photon transitions. The rates of the former transitions, in relativistic calculations, are small due to the strong cancellation contributions to the transition moment (Ynnerman & Fischer 1995), whereas the rates of the latter transitions are identically zero in the simplest approximation of the wave function and only induced by correlation effects (Bogdanovich et al. 2007; Li et al. 2010). These types of transitions are extremely challenging, and therefore interesting from a theoretical point of view, and improved methodology is needed to further decrease the uncertainties of the respective transition data.

Fortunately, the weak transitions tend to be of lesser astrophysical importance, either for opacity calculations, or for spectroscopic abundance analyses. Thus, only the transitions with $A \geq 10^2 \text{ s}^{-1}$ for C I and C II, and $A \geq 10^0 \text{ s}^{-1}$ for C III and C IV, are discussed in the paper; although the complete transition data tables, for all computed E1 transitions in C I–IV, are available online. The scatterplots of dT versus A are given in Fig. 2. The mean dT for all presented E1 transitions shown in Fig. 2 is 8.05% ($\sigma = 0.12$), 7.20% ($\sigma = 0.13$), 1.77% ($\sigma = 0.05$), and 0.28% ($\sigma = 0.0059$), respectively, for C I–IV. A statistical analysis of the proportions of the transitions with dT less than 20%, 10%, and 5% in all the presented E1 transitions is also performed and shown in the last three rows of Table 2.

Finally, the present work can be compared with other theoretical calculations. In Fig. 3, $\log gf$ values from the present work are compared with results from MCHF-BP (Fischer 2006; Tachiev & Fischer 2000, 1999; Fischer et al. 1998), CIV3 (Hibbert et al. 1993; Corrége & Hibbert 2004), and TOPbase data (Cunto & Mendoza 1992), when available. As shown in the figure, the differences between the $\log gf$ values computed in the present work and respective results from other sources are rather small for most of the transitions. Comparing the MCDHF/RCI results with those from CIV3 calculations by Hibbert et al. (1993), which are frequently used in the abundance analyses, 292(228) out of 378 transitions are in agreement within 20% (10%)

Table 2. Distribution of the uncertainties dT (in %) of the computed transition rates in C I–IV depending on the magnitude of the rates. The transition rates are arranged in five groups based on the magnitude of the A values (in s^{-1}). The number of transitions, No., the mean dT , $\langle dT \rangle$, (in %), and the standard deviations, σ , are given for each group of transitions, in C I–IV, respectively. The last three rows show the proportions of the transitions with dT less than 20%, 10%, and 5% in all the transitions with $A \geq 10^2 \text{ s}^{-1}$ for C I and C II and $A \geq 10^0 \text{ s}^{-1}$ for C III and C IV, respectively.

Group	C I			C II			C III			C IV		
	No.	$\langle dT \rangle$ (%)	σ	No.	$\langle dT \rangle$ (%)	σ	No.	$\langle dT \rangle$ (%)	σ	No.	$\langle dT \rangle$ (%)	σ
$< 10^0$	62	52.6	0.34	80	29.6	0.32	137	10.8	0.18	20	5.92	0.061
$10^0 - 10^2$	156	34.0	0.25	134	17.1	0.24	239	5.57	0.096	10	2.38	0.017
$10^2 - 10^4$	451	13.2	0.15	128	14.4	0.19	354	2.48	0.050	6	0.667	0.0047
$10^4 - 10^6$	600	7.20	0.11	167	11.8	0.15	360	1.44	0.034	43	0.267	0.0035
$> 10^6$	284	1.68	0.020	297	1.53	0.023	715	0.297	0.010	307	0.205	0.0041
$dT < 20\%$		87.4%			89.5%			98.4%			100%	
$dT < 10\%$		77.3%			80.7%			95.7%			100%	
$dT < 5\%$		62.0%			68.7%			91.7%			99.4%	

for C I, and 78(66) out of 87 transitions are within the same range for C II. The results from the MCDHF/RCI and MCHF-BP calculations are found to be in very good agreement for C III–IV, with the relative differences being less than 5% for all the computed transitions. More details about the comparisons with other theoretical calculations, as well as with experimental results, are given in Sects 4.1 – 4.4.

4.1 C I

The computed excitation energies, given in Table A1, are compared with results from NIST (Kramida et al. 2019). With the exception of the levels belonging to the $2s2p^3$ configuration, for which the average relative difference between theory and experiment is 1.22%, the mean relative difference for the rest of the states is 0.35%. The complete transition data, for all computed E1 transitions in C I, can be found in Table A2. Based on the statistical analysis of the uncertainties dT shown in table 2, out of the 1335 transitions with $A \geq 10^2 \text{ s}^{-1}$, the proportions of the transitions with dT less than 20%, 10%, and 5% are, respectively, 87.4%, 77.3%, and 62.0%.

In C I, experimental transition data are available for the $2p3p \rightarrow 2p3s$, $2p3d \rightarrow 2p3p$, and $2p4s \rightarrow 2p3p$ transition arrays using a stabilized arc source (Musielok et al. 1997; Golly et al. 2003; Bacawski et al. 2001). In Table A6, the experimental relative line strengths, together with their uncertainties, are compared with the present MCDHF/RCI theoretical values and with values from the non-relativistic CIV3 calculations by Hibbert et al. (1993) that included semi-empirical diagonal energy shifts by LS configuration in the interaction matrix in the determination of the wavefunctions. The estimated uncertainties dT of the MCDHF/RCI line strengths are given as percentages in parentheses. In most cases, the theoretical values fall into, or only slightly outside, the range of the estimated uncertainties of the experimental values.

Comparing the MCDHF/RCI results with the results from the CIV3 calculations by Hibbert et al. (1993), we see that 41 out of the 50 transitions in common are in good agreement, with the relative differences being less than 10% (see Table A6). For the $2p4s^3P^o \rightarrow 2p3p^3P$ transitions and the $2p4s^3P^o_2 \rightarrow 2p3p^3D_1$ transition, the S values deduced from the present MCDHF/RCI calculations differ substantially from the experimental values, i.e., by more than 20%, while the values from the CIV3 calculations appear to be in better agreement with the corresponding experimental values. Based on the agreement between the length and velocity forms, the estimated uncertainties dT of the present MCDHF/RCI calculations for the above-mentioned transitions are of the order of 8.5% and 1.4%, respectively. For the $2p3d^3P^o \rightarrow 2p3p^3P_1$, $2p4s^3P^o_2 \rightarrow 2p3p^3D_2$,

and $2p3d^3D^o_2 \rightarrow 2p3p^3D_3$ transitions, both theoretical results are outside the range of the estimated uncertainties of the experimental values. For the $2p3d^3D^o \rightarrow 2p3p^3P$ transitions, the evaluated relative line strengths by Golly et al. (2003) slightly differ from the observations by Bacawski et al. (2001). The latter seem to be in better overall agreement with the transition rates predicted by the present calculations.

In Table A7, the computed line strengths and transition rates are compared with values from the spline frozen-cores (FCS) method by Zatsarinny & Fischer (2002) and the MCHF-BP calculations by Fischer (2006). Zatsarinny & Fischer (2002) presented oscillator strengths for transitions from the $2p^2^3P$ term to high-lying excited states, while Fischer (2006) considered only transitions from $2p^2^3P$, 1D , and 1S to odd levels up to $2p3d^3P^o$. As seen in the table, the present MCDHF/RCI results seem to be in better agreement with the values from spline FCS calculations. 76 out of 98 transitions from Zatsarinny & Fischer (2002) agree with present values within 10%, while only 38 out of 78 transitions from Fischer (2006) are within the same range. The relatively large differences with Fischer (2006) may be due to the fact that limited electron correlations were included in their calculations. In the MCHF-BP calculations, two types of correlation, i.e., VV, CV, have been accounted for; however, the CC correlation has not been considered. Additionally, CSF expansions obtained from SD substitutions are not as large as the CSF expansions used in the present calculations. For the majority of the strong transitions with $A > 10^6 \text{ s}^{-1}$, there is a very good agreement between the MCDHF/RCI results and the spline FCS values, with the relative difference being less than 5%. On the other hand, for the $2p3d^3F \rightarrow 2p^2^3P$ and $2p4s^1P_1 \rightarrow 2p^2^3P$ transitions, the observed discrepancies between these three methods, i.e., MCDHF/RCI, spline FCS, and MCHF-BP, are quite large. These transitions are all LS -forbidden transitions, the former is with $\Delta L = 2$ and the latter is spin-forbidden transition; these types of transitions are challenging for computations and are always with large uncertainties. For example, for the $2p3d^3F_3 \rightarrow 2p^2^3P_2$ transition, the A values from MCDHF/RCI, spline FCS, and MCHF-BP calculations are, respectively, $7.92\text{E}+06$, $6.24\text{E}+06$, and $1.14\text{E}+07 \text{ s}^{-1}$, with the relative difference between each two of them being greater than 20%. Experimental data are, therefore, needed for validating these theoretical results. On the contrary, based on the agreement between the length and velocity forms displayed in the parentheses, the estimated uncertainties of the MCDHF/RCI calculations for the above-mentioned transitions are all less than 0.5%.

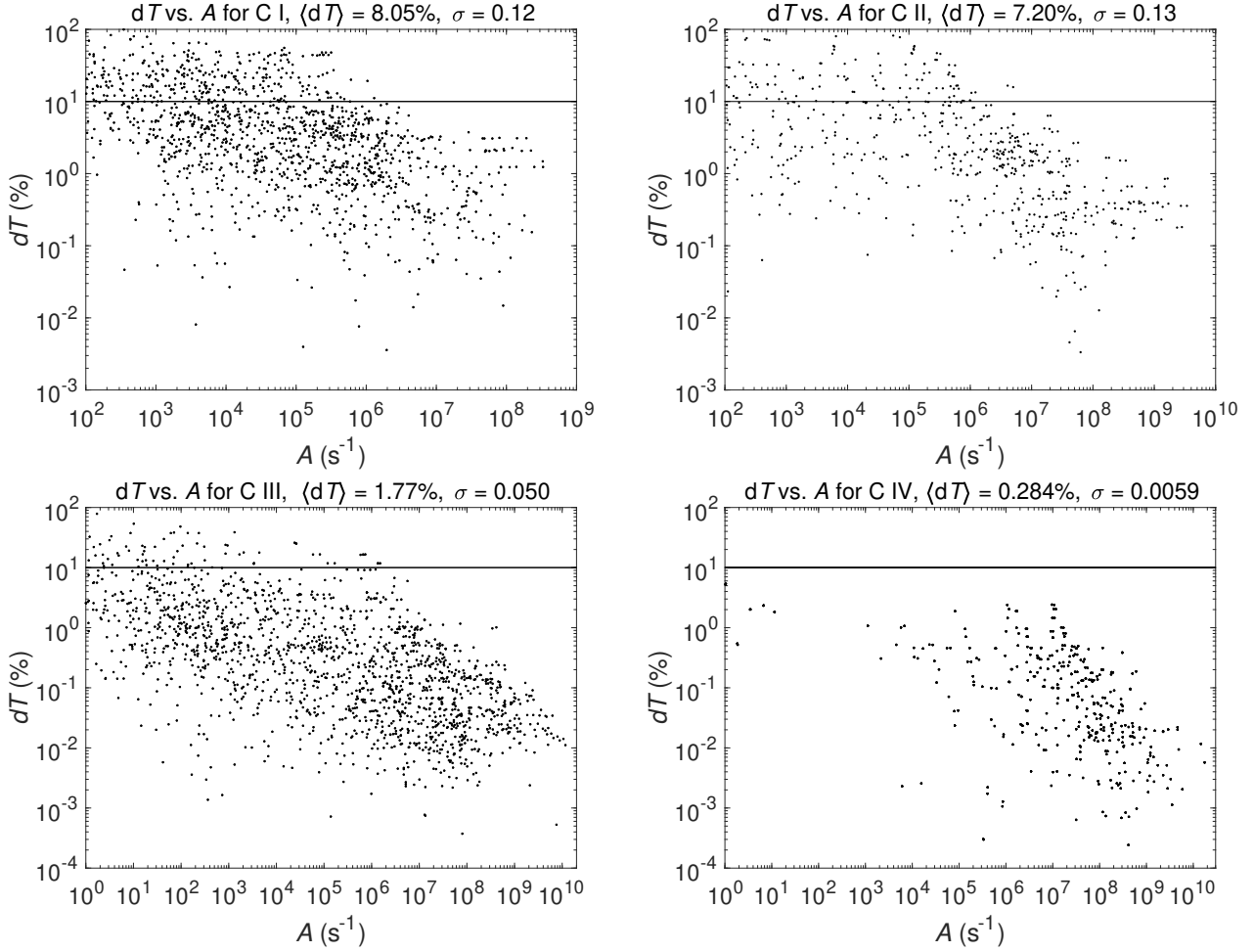


Figure 2. Scatterplot of dT values vs. transition rates A of E1 transitions, for C I–IV. The solid lines indicate the 10% relative agreement between the length and velocity gauges.

4.2 C II

The relative differences between theory and experiment for all the energy levels of $2s2p^2$ are 0.16%, while the mean relative difference for the rest of the states is 0.071% (see Table A1). The complete transition data, for all computed E1 transitions in C II, can be found in Table A3. Out of the presented 592 E1 transitions with $A \geq 10^2 s^{-1}$, the proportions of the transitions with dT less than 20%, 10%, and 5% are, respectively, 89.5%, 80.7%, and 68.7%.

In Table A6, the lifetimes from the present MCDHF/RCI calculations are compared with available results from the MCHF-BP calculations by Tachiev & Fischer (2000) and observations by Reistad et al. (1986) and Träbert et al. (1999). Träbert et al. (1999) measured lifetimes for the three fine-structure components of the $2s2p^2 \ ^4P$ term in an ion storage ring. For the measured lifetimes by Reistad et al. (1986) of the doublets terms using the beam-foil technique, a single value for the two fine-structure levels is provided. It can be seen that, in all cases, the MCDHF/RCI computed lifetimes agree with the experimental values by Reistad et al. (1986) within the experimental errors. For the $2s2p^2 \ ^4P_{1/2,3/2,5/2}$ states, as discussed in Sect. 1, the discrepancies between the measured transition rates by Fang et al. (1993) and by Träbert et al. (1999) are quite large. It is found that the MCDHF/RCI values are in better agreement with the results given by the latter measurements, with a relative difference less than 3%. For

these long-lived states, the measured lifetimes are better represented by the MCDHF/RCI results than by the MCHF-BP values.

The computed line strengths and transition rates are compared with values from the MCHF-BP calculations by Tachiev & Fischer (2000) and the CIV3 calculations by Corrége & Hibbert (2004) in Table A8. We note that the agreement between the present MCDHF/RCI and the MCHF-BP transition rates exhibits a broad variation. In the earlier MCHF-BP and our MCDHF/RCI calculations, the same correlation effects, i.e., VV and CV, have been accounted for. However, the CSF expansions obtained from SD substitutions in the MCHF-BP calculations are not as large as the CSF expansions used in the present calculations, and as a consequence, the LS -composition of the configurations might not be predicted as accurately in the former calculations. The MCDHF/RCI results seem to be in better overall agreement with the values from the CIV3 calculations, except for transitions from $2p^3 \ ^2P^o$ to $2s2p^2 \ \{^4P, ^2S\}$ and to $2s^23d \ ^2D$. For these transitions, involving $2p^3 \ ^2P^o$ as the upper level, the transition rates A are of the order of $10^2 - 10^4 s^{-1}$. The dT values are relatively large in the present calculations. This is due to the strong cancellation effects caused by, e.g., the strong mixing between the $2p^3 \ ^2P^o$ and $2s2p3s \ ^2P^o$ levels for $2p^3 \ ^2P^o \rightarrow 2s2p^2 \ ^2S$, and the mixing between the $2p^3 \ ^2P^o$ and $2s^24p \ ^2P^o$ levels for $2p^3 \ ^2P^o \rightarrow 2s^23d \ ^2D$. Large discrepancies are also observed between the MCDHF/RCI and MCHF-BP results, as well as between the MCHF-BP and CIV3 re-

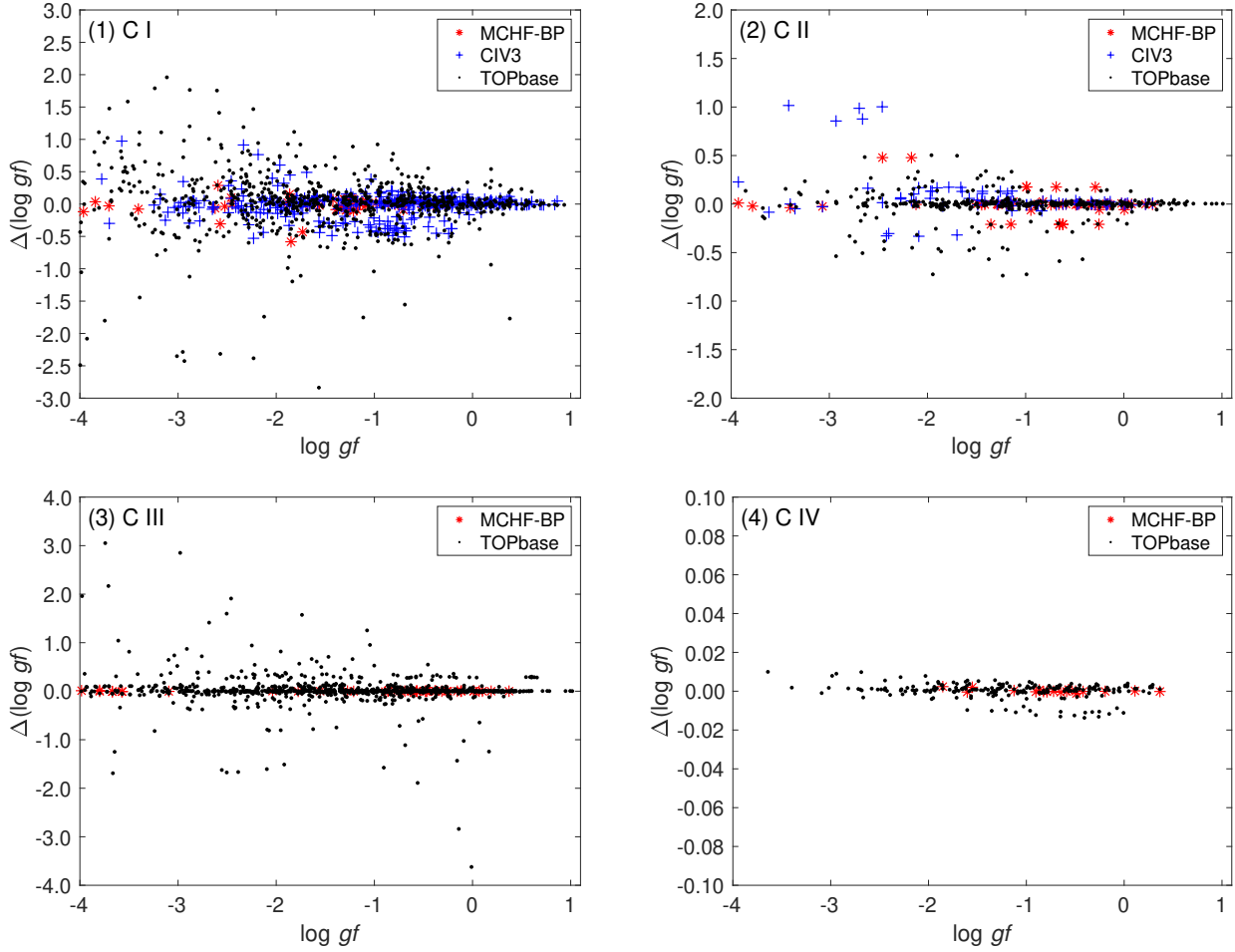


Figure 3. Differences between the calculated $\log gf$ values in this work and results from other theoretical calculations: MCHF-BP (red asterisk), CIV3 (blue plus sign), and TOPbase (black point), for C I–IV.

sults for these transitions. Experimental data are, therefore, crucial for validating the aforementioned theoretical results. On the contrary, for the majority of the strong transitions with $A > 10^6 \text{ s}^{-1}$, there is a very good agreement between the MCDHF/RCI results and those from the two previous calculations, with the relative differences being less than 5%.

4.3 C III

The average relative discrepancy between the computed excitation energies, shown in Table A1, and the NIST recommended values is 0.041%. The complete transition data, for all computed E1 transitions in C III, can be found in Table A4. Out of the 1668 transitions with $A \geq 10^0 \text{ s}^{-1}$, 91.7% (98.4%) of them have dT values less than 5% (20%). Further, the mean dT for all transitions with $A \geq 10^0 \text{ s}^{-1}$ is 1.8% with $\sigma = 0.05$.

The lifetimes of the $2s2p \ ^1P_1^o$, $2p^2 \ \{^1S_0, ^1D_2\}$, and $2s3s \ ^1S_0$ states were measured by Reistad et al. (1986) using the beam-foil technique, and the oscillator strengths for the $2s2p \ ^1P_1^o \rightarrow 2s^2 \ ^1S_0$ and the $2p^2 \ \{^1S_0, ^1D_2\} \rightarrow 2s2p \ ^1P_1^o$ transitions were also provided. Table A6 gives the comparisons between the observed and computed oscillator strengths and lifetimes in C III. Looking at the table, we see an excellent agreement between the present calculations and those from the MCHF-BP calculations (Tachiev & Fischer 1999) with the

relative difference being less than 0.7%. In all cases, the computed oscillator strengths and lifetimes agree with experiment within the experimental errors. The exceptions are the oscillator strength of the $2p^2 \ ^1S_0 \rightarrow 2s2p \ ^1P_1^o$ transition and the lifetime of the $2p^2 \ ^1S_0$ state, for which the computed values slightly differ from the observations.

In Table A9, the computed line strengths and transition rates are compared with values from the MCHF-BP calculations by Tachiev & Fischer (1999) and the GRASP calculations by Aggarwal & Keenan (2015). For the majority of the transitions, there is an excellent agreement between the MCDHF/RCI and MCHF-BP values with the relative differences being less than 1%. Only 4 out of 60 transitions display discrepancies that are greater than 20%. These large discrepancies are observed for the IC transitions, e.g., $2s3d \ ^3D_2 \rightarrow 2s2p \ ^1P_1^o$ and $2s3d \ ^3D_2 \rightarrow 2s2p \ ^1P_1^o$, for which the dT is relatively large. The discrepancies between the MCDHF/RCI and GRASP values are overall large; this is due to the fact that limited electron correlations were included in their calculations. Based on the excellent agreement between the MCDHF/RCI and MCHF-BP results as well as with experiment, we believe that the present transition rates together with the MCHF-BP transition data are more reliable than the ones provided by Aggarwal & Keenan (2015).

4.4 C IV

The mean relative discrepancy between the computed excitation energies, given in Table A1, and the NIST values is 0.0044%. Out of the presented 366 transitions with $A \geq 10^0 \text{ s}^{-1}$ shown in Table A5, only two of them have dT values greater than 5%; 94.0% of them with dT being less than 1%. The mean dT for all transitions with $A \geq 10^0 \text{ s}^{-1}$ is 0.28% with $\sigma = 0.0059$.

For C IV, there are a number of measurements of transition properties. The transition rates of the $2p^2 P_{1/2,3/2}^o \rightarrow 2s^2 S_{1/2}$ transitions were measured by Knystautas et al. (1971) using the beam-foil technique. By using the same technique, the lifetimes for a number of excited states were measured in four different experimental works (Donnelly et al. 1978; Buchet-Poulizac & Buchet 1973b; Jacques et al. 1980; Peach et al. 1988). In Table A6, we compare the theoretical results, from present calculations and MCHF-BP calculations, with the NIST recommended values and observed values. The transition rates of the $2p^2 P_{1/2,3/2}^o \rightarrow 2s^2 S_{1/2}$ transitions from the present work agree perfectly with the values from the MCHF-BP calculations by Fischer et al. (1998), while they are slightly smaller than the NIST data and the values by Knystautas et al. (1971). A comparison of the lifetimes of the $\{3s, 4s, 2p, 3p, 4p, 3d, 4d, 5d\}$ states is made with other theoretical results, i.e., from the MCHF-BP calculations and the Model Potential method. The agreements between these different theoretical results are better than 1% for all these states. Furthermore, the agreement between the computed values and those from observations is also very good except for the $3s^2 S_{1/2}$ level, for which the MCDHF/RCI calculations give a slightly smaller lifetime of 0.2350 ns than the observed value of 0.25 ± 0.01 ns.

In Table A10, the computed line strengths and transition rates are compared with available values from the MCHF-BP calculations by Fischer et al. (1998). There is an excellent agreement between the two methods with the relative differences being less than 1% for all transitions.

5 REANALYSIS OF THE SOLAR CARBON ABUNDANCE

One can also attempt to verify the present atomic data empirically, in an astrophysical context. To demonstrate this, a solar carbon abundance analysis was carried out, based on permitted C I lines. Larger errors in the atomic data usually impart a larger dispersion in the line-by-line abundance results, as well as trends in the results with respect to the line parameters.

The solar carbon abundance analysis recently presented in Amarsi et al. (2019) was taken as the starting point. Their analysis is based on equivalent widths measured in the solar disk-centre intensity, for 14 permitted C I lines in the optical and near-infrared, as well as a single forbidden [C I] line at 872.7 nm. Their analysis draws on a three-dimensional (3D) hydrodynamic model solar atmosphere and 3D non-local thermodynamic equilibrium (non-LTE) radiative transfer, that reflects the current state-of-the-art in stellar elemental abundance determinations (e.g. Asplund et al. 2009). For the 14 permitted C I lines, the authors adopted transition probabilities from NIST, that are based on those of Hibbert et al. (1993) but normalized to a different scale (Haris & Kramida 2017), corresponding to differences of the order ± 0.01 dex.

Here, we post-correct the solar carbon abundances inferred in Amarsi et al. (2019) from the 14 permitted C I lines, using the new atomic data derived in the present study (see Table 3). To first-order, for a given spectral line, the change in the inferred abundances are related to the difference in the adopted transition probabilities

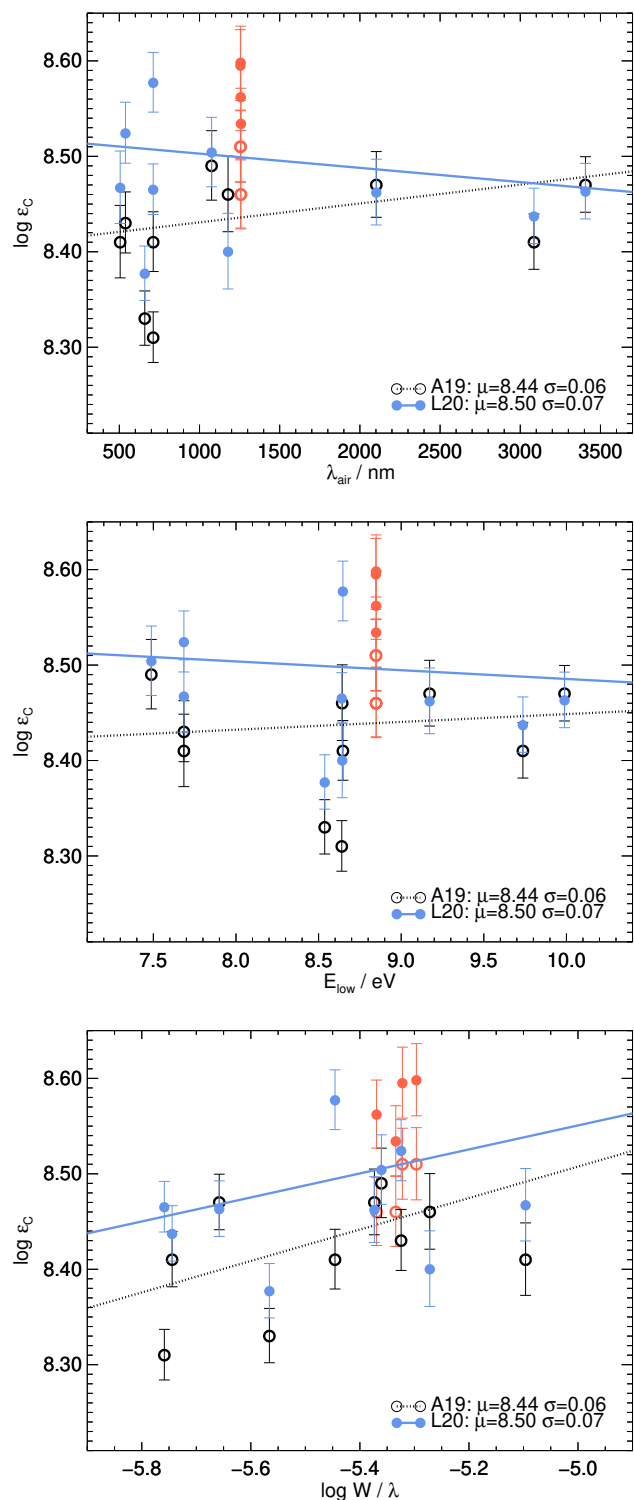


Figure 4. Inferred solar carbon abundances. Black points (A19) are the 3D non-LTE results of Amarsi et al. (2019) for 14 permitted C I lines. Blue points (L20) are these same results but post-corrected using the new $\log gf$ data. Error bars reflect $\pm 5\%$ uncertainties in the measured equivalent widths as stipulated by those authors. The four lines between 1254 nm and 1259 nm discussed in the text have been highlighted in red. The unweighted means μ (including all 14 lines) and the standard deviations of the samples σ are stated in each panel.

Table 3. The 14 permitted C I lines used as abundance diagnostics in Amarsi et al. (2019). Shown are the upper and lower configurations, oscillator strengths obtained from the present calculations, and oscillator strengths from NIST; the latter being based on the calculations from CIV3 (Hibbert et al. 1993). The estimated uncertainties dT of the oscillator strengths are given as percentages in parentheses. The final two columns show the abundances derived in Amarsi et al. (2019), and the post-corrected values derived here based on the formula $\Delta \log \epsilon_C^{\text{line}} = -\Delta \log gf^{\text{line}}$.

Upper	Lower	$\lambda_{\text{air}}(\text{nm})$	$\log gf$		$\log \epsilon_C^{\text{A19}}$	$\log \epsilon_C^{\text{L20}}$
			NIST	MCDHF/RCI(dT)		
2p4p 1D_2	2p3s $^1P_1^o$	505.217	-1.30	-1.36(0.8%)	8.41	8.47
2p4p 1P_1	2p3s $^1P_1^o$	538.034	-1.62	-1.71(1.4%)	8.43	8.52
2p4d $^1P_1^o$	2p3p 1P_1	658.761	-1.00	-1.05(0.2%)	8.33	8.38
2p4d $^3F_2^o$	2p3p 3D_1	711.148	-1.08	-1.24(0.9%)	8.31	8.47
2p4d $^3F_4^o$	2p3p 3D_3	711.318	-0.77	-0.94(1.5%)	8.41	8.58
2p3p 3D_1	2p3s $^3P_2^o$	1075.40	-1.61	-1.62(1.3%)	8.49	8.50
2p3d $^3F_2^o$	2p3p 3D_2	1177.75	-0.52	-0.46(0.9%)	8.46	8.40
2p3d $^3P_1^o$	2p3p 3P_0	1254.95	-0.57	-0.65(3.3%)	8.51	8.60
2p3d $^3P_0^o$	2p3p 3P_1	1256.21	-0.52	-0.61(3.3%)	8.51	8.60
2p3d $^3P_0^o$	2p3p 3P_1	1256.90	-0.60	-0.70(3.2%)	8.46	8.56
2p3d $^3P_2^o$	2p3p 3P_1	1258.16	-0.54	-0.61(3.4%)	8.46	8.53
2p3d $^1P_1^o$	2p3p 1S_0	2102.31	-0.40	-0.39(0.5%)	8.47	8.46
2p4p 1D_2	2p3d $^1F_3^o$	3085.46	+0.10	+0.07(0.2%)	8.41	8.44
2p4d $^1D_2^o$	2p4p 1P_1	3406.58	+0.44	+0.45(3.1%)	8.47	8.46

simply as $\Delta \log \epsilon_C^{\text{line}} = -\Delta \log gf^{\text{line}}$. We briefly note that second-order effects on the inferred abundances, propagated forward from changes to the non-LTE statistical equilibrium when adopting the full set of new $\log gf$ data in the non-LTE model atom, were also tested; these were found to be negligible.

The results of this post-correction are illustrated in Fig. 4. We find that the dispersion in the line-by-line abundance results are similar when using the new and the old sets of $\log gf$ data. We also find that the trends in the results with respect to the line parameters are of similar gradients. This is consistent with the finding in Sect. 4.1, that the precision of this new, much larger atomic data set is comparable to that of Hibbert et al. (1993).

This new analysis implies a solar carbon abundance of 8.50 dex, which is 0.06 dex larger than that inferred in Amarsi et al. (2019) from C I lines, and 0.07 dex larger than the current standard value from Asplund et al. (2009) that is based on C I lines as well as on molecular diagnostics. This increase in the mean abundance is due to 12 of the 14 permitted C I lines having lower oscillator strengths in the present calculations, compared to the NIST data set. Six of the lines give results that are larger than the mean ($\log \epsilon \geq 8.51$); included in this set are all four of the lines between 1254 nm and 1259 nm, which give rise to values of between 8.53 and 8.60 dex. These four lines have the same upper level configuration, 2p3d $^3P^o$, and a closer inspection of the LS -composition reveals that these states are strongly mixed (of the order of 26%) with 2s2p $^3P^o$ states, which are less accurately described in the present calculations. As a consequence, as shown in Table 3, these transitions appear to be associated with slightly larger uncertainties dT than most of the other lines. Omitting these four lines, or adopting NIST oscillator strengths for them, would reduce the mean abundance from 8.50 to 8.47 dex.

Given that the scatter and trends in the results do not support one set of data over the other, we refrain from advocating a higher solar carbon abundance at this point. Nevertheless, this quite drastic change in the resulting solar carbon abundance highlights the importance of having accurate atomic data for abundance analyses. This is especially relevant in the context of the solar modelling problem, wherein standard models of the solar interior, adopting the solar chemical composition of Asplund et al. (2009), fail to reproduce key empirical constraints, including the depth of the convection zone and

interior sound speed that are precisely inferred from helioseismic observations (Basu & Antia 2008; Zhang et al. 2019). Extra opacity in the solar interior near the boundary of the convection zone would resolve the problem (Bailey et al. 2015). Carbon contributes about 5% of the opacity in this region (Blancard et al. 2012), so a higher carbon abundance would help alleviate the problem, albeit only very slightly.

6 CONCLUSIONS

In the present work, energy levels and transition data of E1 transitions are computed for C I–IV using the MCDHF and RCI methods. Special attention is paid to the computation of transition data involving high Rydberg states by employing an alternative orbital optimization approach.

The accuracy of the predicted excitation energies is evaluated by comparing with experimental data provided by the NIST database. The average relative differences of the computed energy levels compared with the NIST data are 0.41%, 0.081%, 0.041%, and 0.0044%, respectively, for C I–IV. The accuracy of the transition data is evaluated based on the relative differences of the computed transition rates in the length and velocity gauges, which is given by the quantity dT , and by extensive comparisons with previous theoretical and experimental results. For most of the strong transitions in C I–IV, the dT values are less than 5%. The mean dT for all presented E1 transitions are 8.05% ($\sigma = 0.12$), 7.20% ($\sigma = 0.13$), 1.77% ($\sigma = 0.050$), and 0.28% ($\sigma = 0.0059$), respectively, for C I–IV. Particularly, for strong transitions with $A > 10^6 \text{ s}^{-1}$, the mean dT is 1.68% ($\sigma = 0.020$), 1.53% ($\sigma = 0.023$), 0.297% ($\sigma = 0.010$), and 0.205% ($\sigma = 0.0041$), respectively, for C I–IV. By employing alternative optimization schemes of the radial orbitals, the uncertainties dT of the computed transition data for transitions involving high Rydberg states are significantly reduced. The agreement between computed transition properties, e.g., line strengths, transition rates, and lifetimes, and experimental values is overall good. The exception is the weak transitions, e.g., the IC transitions, for which the strong cancellation effects are important; however, these effects cannot be properly considered in the present calculations. The present calculations are

extended to high Rydberg states that are not covered by previous accurate calculations and this is of special importance in various astrophysical applications.

The accurate and extensive sets of atomic data for C I–IV are publicly available for use by the astronomy community. These data should be useful for opacity calculations and for models of stellar structures and interiors. They should also be useful to non-LTE spectroscopic analyses of both early-type and late-type stars.

ACKNOWLEDGEMENTS

This work is supported by the Swedish research council under contracts 2015-04842, 2016-04185, 2016-03765, and 2020-03940, and by the Knut and Alice Wallenberg Foundation under the project grant KAW 2013.0052. Some of the computations were enabled by resources provided by the Swedish National Infrastructure for Computing (SNIC) at the Multidisciplinary Center for Advanced Computational Science (UPPMAX) and at the High Performance Computing Center North (HPC2N) partially funded by the Swedish Research Council through grant agreement no. 2018-05973. This work was also supported by computational resources provided by the Australian Government through the National Computational Infrastructure (NCI) under the National Computational Merit Allocation Scheme (NCMAS), under project y89. We thank Nicolas Grevesse for insightful comments on an earlier version of this manuscript. We would also like to thank the anonymous referee for her/his useful comments that helped improve the original manuscript.

DATA AVAILABILITY

The full tables of energy levels (Table A1) and transition data (Tables A2 – A5) are available in the online Supplementary Material.

REFERENCES

- Aggarwal K. M., Keenan F. P., 2015, *Monthly Notices of the Royal Astronomical Society*, 450, 1151
- Alexeeva S., Sadakane K., Nishimura M., Du J., Hu S., 2019, *ApJ*, 884, 150
- Amarsi A. M., Barklem P. S., Collet R., Grevesse N., Asplund M., 2019, *A&A*, 624, A111
- Asplund M., Grevesse N., Sauval A. J., Scott P., 2009, *ARA&A*, 47, 481
- Bacawski A., Wujec T., Musielok J., 2001, *Physica Scripta*, 64, 314
- Bailey J. E., et al., 2015, *Nature*, 517, 56
- Basu S., Antia H. M., 2008, *Phys. Rep.*, 457, 217
- Berkner K., Cooper W., Kaplan S., Pyle R., 1965, *Physics Letters*, 16, 35
- Blancard C., Cossé P., Faussurier G., 2012, *ApJ*, 745, 10
- Bogdanovich P., Karpuškiene R., Rancova O., 2007, *Physica Scripta*, 75, 669
- Boldt G., 1963, *Zeitschrift Naturforschung Teil A*, 18, 1107
- Buchet-Poulizac M. C., Buchet J. P., 1973a, *Physica Scripta*, 8, 40
- Buchet-Poulizac M. C., Buchet J. P., 1973b, *Physica Scripta*, 8, 40
- Caffau E., Ludwig H. G., Bonifacio P., Faraggiana R., Steffen M., Freytag B., Kamp I., Ayres T. R., 2010, *A&A*, 514, A92
- Chen X., et al., 2020, *ApJ*, 889, 157
- Corrége G., Hibbert A., 2004, *Atomic Data and Nuclear Data Tables*, 86, 19
- Cunto W., Mendoza C., 1992, *Rev. Mex. Astron. Astrofis.*, 23, 107
- Cunto W., Mendoza C., Ochsenbein F., Zeippen C. J., 1993, *A&A*, 275, L5
- Doerfert J., Träbert E., Wolf A., Schwalm D., Uwira O., 1997, *Phys. Rev. Lett.*, 78, 4355
- Donnelly K. E., Kernahan J. A., Pinnington E. H., 1978, *J. Opt. Soc. Am.*, 68, 1000
- Dyall K., Grant I., Johnson C., Parpia F., Plummer E., 1989, *Comput. Phys. Commun.*, 55, 425
- Ekman J., Godefroid M., Hartman H., 2014, *Atoms*, 2, 215
- Fang Z., Kwong V. H. S., Wang J., Parkinson W. H., 1993, *Phys. Rev. A*, 48, 1114
- Federman S. R., Zsargo J., 2001, *The Astrophysical Journal*, 555, 1020
- Fischer C. F., 1994, *Physica Scripta*, 49, 323
- Fischer C. F., 2000, *Physica Scripta*, 62, 458
- Fischer C. F., 2006, *Journal of Physics B: Atomic, Molecular and Optical Physics*, 39, 2159
- Fischer C. F., Tachiev G., 2004, *Atomic Data and Nuclear Data Tables*, 87, 1
- Fischer C., Saparov M., Gaigalas G., Godefroid M., 1998, *Atomic Data and Nuclear Data Tables*, 70, 119
- Fischer C. F., Godefroid M., Brage T., Jönsson P., Gaigalas G., 2016, *J. Phys. B: At. Mol. Opt. Phys.*, 49, 182004
- Fischer C. F., Gaigalas G., Jönsson P., Bieroń J., 2019, *Comput. Phys. Commun.*, 237, 184
- Fleming J., Hibbert A., Stafford R. P., 1994, *Physica Scripta*, 49, 316
- Foster E. W., 1962, *Proceedings of the Physical Society*, 79, 94
- Franchini M., et al., 2020, *ApJ*, 888, 55
- Froese Fischer C., 2009, *Physica Scripta Volume T*, 134, 014019
- Fuhr J. R., 2006, *Journal of the American Chemical Society*, 128, 5585
- Gaigalas G., Fischer C. F., Rynkun P., Jönsson P., 2017, *Atoms*, 5
- Godefroid M., Fischer C. F., Jönsson P., 2001, *Journal of Physics B: Atomic, Molecular and Optical Physics*, 34, 1079
- Goldbach C., Nollez G., 1987, *A&A*, 181, 203
- Goldbach C., Martin M., Nollez G., 1989, *A&A*, 221, 155
- Golly A., Jazgara A., Wujec T., 2003, *Physica Scripta*, 67, 485
- Goly A., Weniger S., 1982, *J. Quant. Spectrosc. Radiative Transfer*, 28, 389
- Grant I. P., 1974, *J. Phys. B: At. Mol. Opt. Phys.*, 7, 1458
- Grant I. P., 2007, *Relativistic Quantum Theory of Atoms and Molecules*. Springer, New York
- Haris K., Kramida A., 2017, *The Astrophysical Journal Supplement Series*, 233, 16
- Hibbert A., 1974, *Journal of Physics B: Atomic and Molecular Physics*, 7, 1417
- Hibbert A., 1975, *Computer Physics Communications*, 9, 141
- Hibbert A., Biemont E., Godefroid M., Vaecck N., 1993, *A&AS*, 99, 179
- Jacques C., Knystautas E. J., Drouin R., Berry H. G., 1980, *Canadian Journal of Physics*, 58, 1093
- Jofré P., Jackson H., Tucci Maia M., 2020, *A&A*, 633, L9
- Jones D. W., Wiese W. L., 1984, *Phys. Rev. A*, 29, 2597
- Jönsson P., Gaigalas G., Bieroń J., Fischer C. F., Grant I., 2013, *Comput. Phys. Commun.*, 184, 2197
- Jönsson P., Li J., Gaigalas G., Dong C., 2010, *Atomic Data and Nuclear Data Tables*, 96, 271
- Kingston A. E., Hibbert A., 2000, *Journal of Physics B: Atomic, Molecular and Optical Physics*, 33, 693
- Knystautas E., Barrette L., Neveu B., Drouin R., 1971, *Journal of Quantitative Spectroscopy and Radiative Transfer*, 11, 75
- Kramida A., Yu. Ralchenko Reader J., and NIST ASD Team 2019, NIST Atomic Spectra Database (ver. 5.7.1), [Online]. Available: <https://physics.nist.gov/asd> [2020, February 11]. National Institute of Standards and Technology, Gaithersburg, MD.
- Kwong V. H. S., Fang Z., Gibbons T. T., Parkinson W. H., Smith P. L., 1993, *ApJ*, 411, 431
- Li J., Jönsson P., Dong C., Gaigalas G., 2010, *Journal of Physics B: Atomic, Molecular and Optical Physics*, 43, 035005
- Maecker H., 1953, *Zeitschrift für Physik*, 135, 13
- Mickey D., 1970, *Nuclear Instruments and Methods*, 90, 77
- Miller M. H., Wilkerson T. D., Roig R. A., Bengtson R. D., 1974, *Phys. Rev. A*, 9, 2312
- Moore C. E., Gallagher J. W., 1993, *Tables of spectra of hydrogen, carbon, nitrogen, and oxygen atoms and ions*. Boca Raton : CRC Press
- Musielok J., Veres G., Wiese W., 1997, *Journal of Quantitative Spectroscopy and Radiative Transfer*, 57, 395
- Nandi T., Bhattacharya N., Kurup M. B., Prasad K. G., 1996, *Physica Scripta*, 54, 179
- Nieva M. F., Przybilla N., 2006, *ApJ*, 639, L39
- Nieva M. F., Przybilla N., 2008, *A&A*, 481, 199

- Nieva M. F., Przybilla N., 2012, [A&A](#), **539**, A143
- Nussbaumer H., Storey P. J., 1981, [A&A](#), **96**, 91
- Nussbaumer H., Storey P. J., 1984, [A&A](#), **140**, 383
- Olsen J., Roos B. O., Jørgensen P., Jensen H. J. A., 1988, [J. Chem. Phys.](#), **89**, 2185
- Papoulia A., et al., 2019, *Atoms*, 7
- Peach G., Saraph H. E., Seaton M. J., 1988, [Journal of Physics B: Atomic, Molecular and Optical Physics](#), **21**, 3669
- Pehlivan Rhodin A., Hartman H., Nilsson H., Jönsson P., 2017, [A&A](#), **598**, A102
- Przybilla N., Butler K., Kudritzki R. P., 2001, [A&A](#), **379**, 936
- Reistad N., Martinson I., 1986, [Phys. Rev. A](#), **34**, 2632
- Reistad N., Hutton R., Nilsson A. E., Martinson I., Mannervik S., 1986, [Physica Scripta](#), **34**, 151
- Richter J., 1958, [Zeitschrift für Physik](#), **151**, 114
- Roberts J. R., Eckerle K. L., 1967, [Phys. Rev.](#), **153**, 87
- Stonkutė E., et al., 2020, [AJ](#), **159**, 90
- Sturesson L., Jönsson P., Froese Fischer C., 2007, [CoPhC](#), **177**, 539
- Tachiev G., Fischer C. F., 1999, [Journal of Physics B: Atomic, Molecular and Optical Physics](#), **32**, 5805
- Tachiev G., Fischer C. F., 2000, [Journal of Physics B: Atomic, Molecular and Optical Physics](#), **33**, 2419
- Tachiev G., Fischer C. F., 2001, [Canadian Journal of Physics](#), **79**, 955
- Träbert E., Gwinner G., Knystautas E. J., Tordoir X., Wolf A., 1999, [Journal of Physics B: Atomic, Molecular and Optical Physics](#), **32**, L491
- VandenBerg D. A., Bergbusch P. A., Dotter A., Ferguson J. W., Michaud G., Richer J., Proffitt C. R., 2012, [ApJ](#), **755**, 15
- Wiese W. L., Fuhr J. R., 2007a, [Journal of Physical and Chemical Reference Data](#), **36**, 1287
- Wiese W. L., Fuhr J. R., 2007b, [Journal of Physical and Chemical Reference Data](#), **36**, 1737
- Ynnerman A., Fischer C. F., 1995, [Phys. Rev. A](#), **51**, 2020
- Zatsarinny O., Fischer C. F., 2002, [Journal of Physics B: Atomic, Molecular and Optical Physics](#), **35**, 4669
- Zhang Q.-S., Li Y., Christensen-Dalsgaard J., 2019, [ApJ](#), **881**, 103

APPENDIX A: ADDITIONAL TABLES

Table A1. Wave function composition (up to three LS components with a contribution > 0.02 of the total wave function) in LS -coupling, energy levels (in cm^{-1}), and lifetimes (in s; given in length (τ_l) and velocity (τ_v) gauges) for C I–IV. Energy levels are given relative to the ground state and compared with NIST data (Kramida et al. 2019). The full table is available online.

Species	No.	State	LS -composition	E_{RCI}	E_{NIST}	τ_l	τ_v
C I	1	$2s^2 2p^2 (^3P) ^3P_0$	$0.88 + 0.03 2s^2 2p^2 ^2P ^3P$	0	0		
C I	2	$2s^2 2p^2 (^3P) ^3P_1$	$0.88 + 0.03 2s^2 2p^2 ^2P ^3P$	16	16		
C I	3	$2s^2 2p^2 (^3P) ^3P_2$	$0.88 + 0.03 2s^2 2p^2 ^2P ^3P$	43	43		
C I	4	$2s^2 2p^2 (^1D) ^1D_2$	$0.85 + 0.05 2s^2 2p^2 ^2P ^1D + 0.03 2s^2 2p^2 ^2P ^3P ^1D$	10 275	10 193		
C I	5	$2s^2 2p^2 (^1S) ^1S_0$	$0.78 + 0.06 2s^2 2p^2 ^2P ^1S + 0.06 2p^4 (^1S) ^1S$	21 775	21 648		
C I	6	$2s^2 S 2p^3 (^4S) ^5S^{\circ}_2$	$0.93 + 0.04 2s^2 S 2p^2 (^3P) ^4P ^5S^{\circ}$	33 859	33 735	3.00E-02	1.26E-02
C I	7	$2s^2 2p^2 ^2P ^3s ^3P^{\circ}_0$	$0.91 + 0.04 2p^3 (^2P) ^2P ^3s ^3P^{\circ}$	60 114	60 333	3.00E-09	3.04E-09
C I	8	$2s^2 2p^2 ^2P ^3s ^3P^{\circ}_1$	$0.91 + 0.04 2p^3 (^2P) ^2P ^3s ^3P^{\circ}$	60 133	60 353	3.00E-09	3.04E-09
C I	9	$2s^2 2p^2 ^2P ^3s ^3P^{\circ}_2$	$0.91 + 0.04 2p^3 (^2P) ^2P ^3s ^3P^{\circ}$	60 174	60 393	3.00E-09	3.04E-09
C I	10	$2s^2 2p^2 ^2P ^3s ^1P^{\circ}_1$	$0.92 + 0.04 2p^3 (^2P) ^2P ^3s ^1P^{\circ}$	61 750	61 982	2.78E-09	2.83E-09
–	–	–	–	–	–	–	–

Table A2. Electric dipole transition data for C I from present calculations. Upper and lower states, wavenumber, ΔE , wavelength, λ , line strength, S , weighted oscillator strength, gf , transition probability, A , together with the relative difference between two gauges of A values, dT , provided by the present MCDHF/RCI calculations are shown in the table. Wavelength and wavenumber values are from the NIST database (Kramida et al. 2019) when available. Wavelengths and wavenumbers marked with * are from the present calculations. Only the first ten rows are shown; the full table is available online.

Upper	Lower	$\Delta E(\text{cm}^{-1})$	$\lambda(\text{\AA})$	$S(\text{a.u. of } a_0^2 e^2)$	gf	$A(\text{s}^{-1})$	dT
$2s^2 2p 5d ^3D^{\circ}_2$	$2s^2 2p^2 ^3P_1$	86373	1157.769	1.025E-01	2.679E-02	2.647E+07	0.004
$2s^2 2p 5d ^3D^{\circ}_1$	$2s^2 2p^2 ^3P_0$	86362	1157.909	8.568E-02	2.240E-02	3.689E+07	0.003
$2s^2 2p 5d ^3D^{\circ}_3$	$2s^2 2p^2 ^3P_2$	86354	1158.018	3.197E-01	8.358E-02	5.897E+07	0.003
$2s^2 2p 6s ^3P^{\circ}_2$	$2s^2 2p^2 ^3P_1$	86352	1158.038	1.273E-01	3.328E-02	3.287E+07	0.002
$2s^2 2p 5d ^3D^{\circ}_1$	$2s^2 2p^2 ^3P_1$	86346	1158.130	4.687E-02	1.225E-02	2.017E+07	0.002
$2s^2 2p 5d ^3D^{\circ}_2$	$2s^2 2p^2 ^3P_2$	86346	1158.131	1.049E-01	2.742E-02	2.708E+07	0.000
$2s^2 2p 6s ^3P^{\circ}_1$	$2s^2 2p^2 ^3P_0$	86331	1158.324	2.442E-02	6.380E-03	1.050E+07	0.001
$2s^2 2p 6s ^3P^{\circ}_2$	$2s^2 2p^2 ^3P_2$	86325	1158.400	2.619E-02	6.844E-03	6.756E+06	0.001
$2s^2 2p 5d ^3D^{\circ}_1$	$2s^2 2p^2 ^3P_2$	86319	1158.492	1.367E-03	3.571E-04	5.875E+05	0.002
$2s^2 2p 6s ^3P^{\circ}_1$	$2s^2 2p^2 ^3P_1$	86315	1158.544	6.630E-03	1.732E-03	2.849E+06	0.004
–	–	–	–	–	–	–	–

Table A3. Electric dipole transition data for C II from present calculations. Upper and lower states, wavenumber, ΔE , wavelength, λ , line strength, S , weighted oscillator strength, gf , transition probability, A , together with the relative difference between two gauges of A values, dT , provided by the present MCDHF/RCI calculations are shown in the table. Wavelength and wavenumber values are from the NIST database (Kramida et al. 2019) when available. Only the first ten rows are shown; the full table is available online.

Upper	Lower	$\Delta E(\text{cm}^{-1})$	$\lambda(\text{\AA})$	$S(\text{a.u. of } a_0^2 e^2)$	gf	$A(\text{s}^{-1})$	dT
$2s 2p 3p ^2D_{3/2}$	$2s^2 2p ^2P^{\circ}_{1/2}$	188581	530.275	8.159E-02	4.673E-02	2.771E+08	0.015
$2s 2p 3p ^2D_{5/2}$	$2s^2 2p ^2P^{\circ}_{3/2}$	188551	530.359	1.515E-01	8.678E-02	3.430E+08	0.015
$2s 2p 3p ^2D_{3/2}$	$2s^2 2p ^2P^{\circ}_{3/2}$	188517	530.454	1.661E-02	9.511E-03	5.636E+07	0.015
$2s^2 7d ^2D_{3/2}$	$2s^2 2p ^2P^{\circ}_{1/2}$	187353	533.752	1.094E-01	6.223E-02	3.637E+08	0.007
$2s^2 7d ^2D_{5/2}$	$2s^2 2p ^2P^{\circ}_{3/2}$	187289	533.933	1.943E-01	1.104E-01	4.300E+08	0.007
$2s^2 7d ^2D_{3/2}$	$2s^2 2p ^2P^{\circ}_{3/2}$	187289	533.933	2.205E-02	1.254E-02	7.321E+07	0.007
$2s 2p 3p ^4P_{3/2}$	$2s^2 2p ^2P^{\circ}_{1/2}$	186443	536.355	1.779E-07	1.007E-07	5.830E+02	0.017
$2s 2p 3p ^4P_{1/2}$	$2s^2 2p ^2P^{\circ}_{1/2}$	186427	536.402	6.007E-07	3.400E-07	3.936E+03	0.039
$2s 2p 3p ^4P_{5/2}$	$2s^2 2p ^2P^{\circ}_{3/2}$	186402	536.473	1.227E-05	6.942E-06	2.678E+04	0.020
$2s 2p 3p ^4P_{3/2}$	$2s^2 2p ^2P^{\circ}_{3/2}$	186380	536.537	1.327E-06	7.506E-07	4.343E+03	0.027
–	–	–	–	–	–	–	–

Table A4. Electric dipole transition data for C III from present calculations. Upper and lower states, wavenumber, ΔE , wavelength, λ , line strength, S , weighted oscillator strength, gf , transition probability, A , together with the relative difference between two gauges of A values, dT , provided by the present MCDHF/RCI calculations are shown in the table. Wavelength and wavenumber values are from the NIST database (Kramida et al. 2019) when available. Wavelengths and wavenumbers marked with * are from the present calculations. Only the first ten rows are shown; the full table is available online.

Upper	Lower	$\Delta E(\text{cm}^{-1})$	$\lambda (\text{\AA})$	$S (\text{a.u. of } a_0^2 e^2)$	gf	$A (\text{s}^{-1})$	dT
2s7p $^3\text{P}_1^o$	2s 2 $^1\text{S}_0$	365034*	273.947*	7.670E-07	8.505E-07	2.520E+04	0.005
2s7p $^1\text{P}_1^o$	2s 2 $^1\text{S}_0$	364896	274.051	1.043E-02	1.156E-02	3.423E+08	0.010
2s6p $^1\text{P}_1^o$	2s 2 $^1\text{S}_0$	357109	280.026	1.593E-02	1.728E-02	4.901E+08	0.001
2s6p $^3\text{P}_1^o$	2s 2 $^1\text{S}_0$	357050	280.073	5.265E-06	5.711E-06	1.619E+05	0.004
2p3d $^1\text{P}_1^o$	2s 2 $^1\text{S}_0$	346712	288.423	9.317E-04	9.818E-04	2.627E+07	0.003
2s5p $^3\text{P}_1^o$	2s 2 $^1\text{S}_0$	344236	290.498	3.900E-07	4.079E-07	1.075E+04	0.018
2s5p $^1\text{P}_1^o$	2s 2 $^1\text{S}_0$	343258	291.326	4.551E-02	4.747E-02	1.244E+09	0.000
2p3d $^3\text{P}_1^o$	2s 2 $^1\text{S}_0$	340127	294.007	7.645E-07	7.903E-07	2.035E+04	0.005
2p3d $^3\text{D}_1^o$	2s 2 $^1\text{S}_0$	337655	296.159	7.267E-07	7.458E-07	1.893E+04	0.005
2s4p $^1\text{P}_1^o$	2s 2 $^1\text{S}_0$	322404	310.170	3.480E-02	3.409E-02	7.884E+08	0.000
–	–	–	–	–	–	–	–

Table A5. Electric dipole transition data for C IV from present calculations. Upper and lower states, wavenumber, ΔE , wavelength, λ , line strength, S , weighted oscillator strength, gf , transition probability, A , together with the relative difference between two gauges of A values, dT , provided by the present MCDHF/RCI calculations are shown in the table. Wavelength and wavenumber values are from the NIST database (Kramida et al. 2019). Only the first ten rows are shown; the full table is available online.

Upper	Lower	$\Delta E(\text{cm}^{-1})$	$\lambda (\text{\AA})$	$S (\text{a.u. of } a_0^2 e^2)$	gf	$A (\text{s}^{-1})$	dT
8p $^2\text{P}_{3/2}^o$	2s $^2\text{S}_{1/2}$	492479	203.054	5.029E-03	7.523E-03	3.043E+08	0.004
8p $^2\text{P}_{1/2}^o$	2s $^2\text{S}_{1/2}$	492477	203.055	2.517E-03	3.766E-03	3.046E+08	0.004
7p $^2\text{P}_{3/2}^o$	2s $^2\text{S}_{1/2}$	483950	206.633	7.885E-03	1.159E-02	4.527E+08	0.001
7p $^2\text{P}_{1/2}^o$	2s $^2\text{S}_{1/2}$	483948	206.634	3.946E-03	5.801E-03	4.532E+08	0.001
6p $^2\text{P}_{3/2}^o$	2s $^2\text{S}_{1/2}$	470778	212.414	1.349E-02	1.930E-02	7.132E+08	0.000
6p $^2\text{P}_{1/2}^o$	2s $^2\text{S}_{1/2}$	470775	212.416	6.753E-03	9.657E-03	7.139E+08	0.000
5p $^2\text{P}_{3/2}^o$	2s $^2\text{S}_{1/2}$	448862	222.785	2.644E-02	3.604E-02	1.211E+09	0.000
5p $^2\text{P}_{1/2}^o$	2s $^2\text{S}_{1/2}$	448855	222.789	1.323E-02	1.804E-02	1.212E+09	0.000
8d $^2\text{D}_{3/2}$	2p $^2\text{P}_{1/2}^o$	428244	233.511	1.264E-02	1.644E-02	5.027E+08	0.002
8d $^2\text{D}_{5/2}$	2p $^2\text{P}_{3/2}^o$	428136	233.570	2.275E-02	2.958E-02	6.028E+08	0.002
–	–	–	–	–	–	–	–

Table A6. Comparison of relative line strengths (S), weighted oscillator strengths (gf), and lifetimes (τ), or transition probabilities (A), with other theoretical work and experimental results for C I–IV. The present values from the MCDHF/RCI calculations are given in the Babushkin(length) gauge. The values in the parentheses are the relative differences between the length and velocity gauges. The references for the experiments are shown in the last column. Note that the sums of the line strengths S have been normalized to 100 for each multiplet in C I.

C I						
Transition array	Mult.	$J_u - J_l$	S (a.u. of $a_0^2 e^2$)			
			MCDHF/RCI	CIV3 ^(a)	Expt.	Expt.
$2s^2 2p3p - 2s^2 2p3s$	$^3D - ^3P^o$	3 - 2	46.67(1.3%)	46.72	46.3 ± 1.8 ^(b)	
		2 - 1	25.29(1.2%)	25.43	25.5 ± 1.2 ^(b)	
		1 - 0	11.25(1.2%)	11.29	11.8 ± 0.5 ^(b)	
		2 - 2	8.047(1.3%)	7.898	7.67 ± 0.38 ^(b)	
		1 - 1	8.213(1.3%)	8.153	8.42 ± 0.46 ^(b)	
$2s^2 2p3p - 2s^2 2p3s$	$^3P - ^3P^o$	2 - 2	42.15(0.2%)	41.92	40.6 ± 0.9 ^(b)	41.3 ^(d)
		1 - 1	7.812(0.3%)	7.873	7.98 ± 0.23 ^(b)	8.1 ^(d)
		1 - 2	15.07(0.2%)	14.79	15.1 ± 0.4 ^(b)	15.1 ^(d)
		0 - 1	11.11(0.2%)	11.11	11.3 ± 0.3 ^(b)	11.6 ^(d)
		2 - 1	13.41(0.2%)	13.67	14.0 ± 0.35 ^(b)	13.0 ^(d)
		1 - 0	10.44(0.2%)	10.64	10.9 ± 0.3 ^(b)	10.9 ^(d)
		1 - 2	51.96(0.3%)	51.43	52.4 ± 1.1 ^(b)	
$2s^2 2p3p - 2s^2 2p3s$	$^3S - ^3P^o$	1 - 1	35.49(0.2%)	35.80	34.8 ± 0.9 ^(b)	
		1 - 0	12.54(0.2%)	12.77	12.8 ± 0.38 ^(b)	
		2 - 1	57.27(3.0%)	56.85	59.0 ± 3.2 ^(c)	
$2s^2 2p3d - 2s^2 2p3p$	$^3P^o - ^3S$	1 - 1	32.30(2.9%)	32.56	32.1 ± 4.1 ^(c)	
		0 - 1	10.43(2.9%)	10.59	8.9 ± 2.1 ^(c)	
		2 - 2	42.67(3.3%)	42.63	43.5 ± 0.4 ^(c)	
$2s^2 2p3d - 2s^2 2p3p$	$^3P^o - ^3P$	1 - 1	9.465(3.2%)	9.669	10.2 ± 0.6 ^(c)	
		1 - 2	13.91(3.3%)	13.84	14.9 ± 0.8 ^(c)	
		0 - 1	11.57(3.3%)	11.69	11.2 ± 0.5 ^(c)	
		2 - 1	11.72(3.4%)	11.47	10.2 ± 0.5 ^(c)	
		1 - 0	10.66(3.3%)	10.70	10.0 ± 0.4 ^(c)	
		2 - 2	62.05(5.7%)	50.76	51.2 ± 5.0 ^(c)	
		1 - 1	9.312(7.1%)	8.778	8.4 ± 1.6 ^(c)	
$2s^2 2p4s - 2s^2 2p3p$	$^3P^o - ^3P$	1 - 2	13.79(7.0%)	14.08	14.3 ± 2.0 ^(c)	
		0 - 1	7.335(8.7%)	9.670	10.2 ± 1.5 ^(c)	
		2 - 1	3.113(11.9%)	8.440	10.1 ± 2.0 ^(c)	
		1 - 0	4.397(10.3%)	8.271	5.8 ± 1.0 ^(c)	
		3 - 2	47.89(1.2%)	46.50	45.5 ± 2.0 ^(c)	45.1 ^(d)
		2 - 1	26.70(1.2%)	26.59	27.5 ± 1.2 ^(c)	24.2 ^(d)
		1 - 0	9.708(1.2%)	11.11	11.0 ± 0.6 ^(c)	13.6 ^(d)
$2s^2 2p3d - 2s^2 2p3p$	$^3D^o - ^3P$	2 - 2	8.170(0.9%)	7.559	7.5 ± 0.4 ^(c)	8.0 ^(d)
		1 - 1	7.100(1.1%)	7.792	8.1 ± 0.5 ^(c)	9.1 ^(d)
		2 - 3	44.42(3.2%)	44.77	44.5 ± 2.0 ^(c)	
		1 - 2	23.65(3.1%)	24.14	24.8 ± 1.2 ^(c)	
		0 - 1	11.10(3.0%)	11.24	11.5 ± 0.6 ^(c)	
		2 - 2	9.145(2.6%)	9.424	8.4 ± 0.6 ^(c)	
		1 - 1	9.301(2.7%)	9.071	9.5 ± 0.5 ^(c)	
$2s^2 2p4s - 2s^2 2p3p$	$^3P^o - ^3D$	2 - 1	2.373(1.4%)	1.356	1.3 ± 0.2 ^(c)	
		3 - 3	50.31(1.5%)	49.19	50.0 ± 5.0 ^(c)	
		2 - 2	25.28(1.6%)	25.72	25.4 ± 2.2 ^(c)	
		1 - 1	11.50(1.7%)	12.68	12.3 ± 0.7 ^(c)	
		2 - 3	8.250(0.9%)	7.291	6.6 ± 0.6 ^(c)	
		1 - 2	4.043(1.8%)	4.621	4.7 ± 0.5 ^(c)	
		4 - 3	43.41(0.4%)	43.53	44.9 ± 2.0 ^(c)	
$2s^2 2p3d - 2s^2 2p3p$	$^3F^o - ^3D$	3 - 2	30.86(0.4%)	30.92	30.0 ± 1.5 ^(c)	
		2 - 1	20.77(0.3%)	21.09	20.4 ± 1.0 ^(c)	
		3 - 3	1.961(1.2%)	1.743	1.9 ± 0.2 ^(c)	
		3 - 3	1.961(1.2%)	1.743	1.9 ± 0.2 ^(c)	

		2 - 2	2.999(0.9%)	2.722	2.7±0.2 ^(c)		
C II							
Configuration	Term	<i>J</i>	τ (ns)			Ref.	
			MCDHF/RCI	MCHF-BP ^(e)	Expt.		
2s2p ²	² S	1/2	0.4497 (0.7%)	0.4523	0.44± 0.02	(f)	
2s ² 3s	² S	1/2	2.292 (0.6%)	2.266	2.4 ± 0.3	(f)	
2s ² 4s	² S	1/2	2.017 (0.1%)		1.9 ± 0.1	(f)	
2s ² 5s	² S	1/2	3.774 (0.1%)		3.7 ± 0.2	(f)	
2s2p ²	² P ^o	1/2	0.2446(0.3%)	0.2445	0.25± 0.01	(f)	
		3/2	0.2445(0.3%)	0.2449	0.25± 0.01	(f)	
2s ² 3p	² P ^o	1/2	9.265(0.7%)	8.973	8.9 ± 0.4	(f)	
		3/2	9.255(0.7%)	8.963	8.9 ± 0.4	(f)	
2s ² 4p	² P ^o	1/2	3.838(1.3%)		3.8 ± 0.2	(f)	
		3/2	3.854(1.3%)		3.8 ± 0.2	(f)	
2p ³	² P ^o	1/2	0.4998(0.8%)	0.4966	0.48± 0.02	(f)	
		3/2	0.4981(0.8%)	0.4944	0.48± 0.02	(f)	
2s ² 5p	² P ^o	1/2	5.044(0.2%)		5.2 ± 0.3	(f)	
		3/2	5.099(0.2%)		5.2 ± 0.3	(f)	
2s ² 3d	² D	3/2	0.3490(0.2%)	0.3493	0.34± 0.01	(f)	
		5/2	0.3491(0.2%)	0.3494	0.34± 0.01	(f)	
2s ² 4d	² D	3/2	0.7299(0.2%)		0.75± 0.03	(f)	
		5/2	0.7304(0.2%)		0.75± 0.03	(f)	
Configuration	Term	<i>J</i>	τ (ms)			Ref.	
			MCDHF/RCI	MCHF-BP ^(e)	Expt.		
2s2p ²	⁴ P	1/2	8.151 (47.6%)	7.654	7.95±0.07	(g)	
		3/2	106.1 (68.5%)	96.93	104.1±0.5	(g)	
		5/2	22.66 (48.0%)	22.34	22.05±0.07	(g)	
C III							
Transition array	Mult.	<i>J_u - J_l</i>	<i>gf</i>			Ref.	
			MCDHF/RCI	MCHF-BP ^(h)	Expt.		
2s2p - 2s ²	¹ P ^o - ¹ S	1-0	0.7592(0.1%)	0.7583	0.75 ± 0.03	(f)	
2p ² - 2s2p	¹ S - ¹ P ^o	0-1	0.1623(<0.05%)	0.1622	0.152 ± 0.009	(f)	
2p ² - 2s2p	¹ D - ¹ P ^o	2-1	0.1815(0.5%)	0.1819	0.183 ± 0.005	(f)	
Configuration	Term	<i>J</i>	τ (ns)			Ref.	
			MCDHF/RCI	MCHF-BP ^(h)	Expt.		
2s2p	¹ P ^o	1	0.5638(0.1%) ns	0.5651	0.57± 0.02	(f)	
2p ²	¹ S	0	0.4766(<0.05%) ns	0.4764	0.51± 0.01	(f)	
2p ²	¹ D	2	7.240(0.5%) ns	7.191	7.2± 0.2	(f)	
2s3s	¹ S	0	1.164(<0.05%) ns	1.171	1.17± 0.05	(f)	
C IV							
Transition array	Mult.	<i>J_u - J_l</i>	<i>A</i> (10 ⁸ s ⁻¹)				Ref.
			MCDHF/RCI	MCHF-BP ^(j)	NIST	Expt.	
2p - 2s	² P ^o - ² S	1/2 - 1/2	2.632(<0.05%)	2.6320	2.65	2.72±0.07	(k)
2p - 2s	² P ^o - ² S	3/2 - 1/2	2.646(<0.05%)	2.6459	2.64	2.71±0.07	(k)
Configuration	Term	<i>J</i>	τ (ns)			Ref.	
			MCDHF/RCI	MCHF-BP ^(j)	Model Potential ^(o)		Expt.
3s	² S	1/2	0.2350(<0.05%)	0.2350	0.236	0.25 ± 0.1	(l)
4s	² S	1/2	0.3755(<0.05%)	0.3747	0.377	0.34 ± 0.035	(m)
2p	² P ^o	1/2	3.799 (<0.05%)	3.799	3.79	3.7 ± 0.1	(k)
		3/2	3.779 (<0.05%)	3.779	3.79		
3p	² P ^o	1/2	0.2146(<0.05%)	0.2142	0.216	0.226 ± 0.03	(n)

4p	2°P	3/2	0.2149(<0.05%)	0.2145	0.216	0.32 ± 0.03	(m)
		1/2	0.3435(<0.05%)		0.344		
		3/2	0.3440(<0.05%)		0.344		
3d	2°D	3/2	0.05717(<0.05%)	0.05716	0.0572	0.0575 ± 0.006	(n)
		5/2	0.05719(<0.05%)	0.05719	0.0572		
4d	2°D	3/2	0.1312 (<0.05%)		0.130	0.14 ± 0.015	(m)
		5/2	0.1313 (<0.05%)		0.130		
5d	2°D	3/2	0.2511 (<0.05%)		0.251	0.23 ± 0.023	(m)
		5/2	0.2512 (<0.05%)		0.251		

(*a*) Hibbert et al. (1993); (*b*) Musielok et al. (1997); (*c*) Bacawski et al. (2001); (*d*) Golly et al. (2003); (*e*) Tachiev & Fischer (2000); (*f*) Reistad et al. (1986); (*g*) Träbert et al. (1999); (*h*) Tachiev & Fischer (1999); (*j*) Fischer et al. (1998); (*k*) Knystautas et al. (1971); (*l*) Donnelly et al. (1978); (*m*) Buchet-Poulizac & Buchet (1973b); (*n*) Jacques et al. (1980); (*o*) Peach et al. (1988).

Table A7. Comparison of line strengths (S) and transition rates (A) with other theoretical results for C I. The present values from the MCDHF/RCI calculations are given in the Babushkin(length) gauge. The wavenumber ΔE and wavelength λ values are taken from the NIST database. The estimated uncertainties dT of the transition rates are given as percentages in parentheses.

Transition array	Mult.	$J_u - J_l$	ΔE (cm ⁻¹)	λ (Å)	MCDHF/RCI		Spline FCS(<i>a</i>)		MCHF-BP(<i>b</i>)	
					S (a.u. of $a_0^2 e^2$)	A (s ⁻¹)	S (a.u. of $a_0^2 e^2$)	A (s ⁻¹)	S (a.u. of $a_0^2 e^2$)	A (s ⁻¹)
$2s^2 2p3d - 2s^2 2p^2$	$3^{\circ}\text{F}^{\circ} - 3^{\circ}\text{P}$	3 - 2	78172	1279.228	5.79E-02	7.92E+06(0.1%)	4.52E-02	6.24E+06	8.20E-02	1.14E+07
		2 - 2	78155	1279.498	1.27E-02	2.43E+06(0.3%)	9.62E-03	1.86E+06	1.16E-02	2.25E+06
		2 - 1	78182	1279.056	1.08E-02	2.07E+06(0.1%)	8.95E-03	1.73E+06	2.08E-02	4.04E+06
$2s^2 2p4d - 2s^2 2p^2$	$3^{\circ}\text{F}^{\circ} - 3^{\circ}\text{P}$	3 - 2	83717	1194.488	4.48E-02	7.52E+06(0.1%)	3.99E-02	6.77E+06		
		2 - 2	83709	1194.614	1.59E-03	3.74E+05(0.5%)	1.44E-03	3.42E+05		
		2 - 1	83736	1194.229	1.97E-02	4.64E+06(0.2%)	1.73E-02	4.10E+06		
$2s^2 2p5d - 2s^2 2p^2$	$3^{\circ}\text{F}^{\circ} - 3^{\circ}\text{P}$	3 - 2	86283	1158.966	4.17E-02	7.67E+06(0.3%)	3.88E-02	7.21E+06		
		2 - 2	86274	1159.094	1.38E-03	3.55E+05(0.3%)	1.36E-03	3.54E+05		
		2 - 1	86301	1158.731	2.20E-02	5.66E+06(0.3%)	1.96E-02	5.11E+06		
$2s^2 2p3s - 2s^2 2p^2$	$3^{\circ}\text{P}^{\circ} - 3^{\circ}\text{P}$	2 - 2	60349	1657.008	2.84E+00	2.50E+08(1.2%)	2.69E+00	2.41E+08	2.93E+00	2.61E+08
		1 - 2	60309	1658.121	9.46E-01	1.39E+08(1.2%)	8.95E-01	1.33E+08	9.75E-01	1.45E+08
		2 - 1	60376	1656.267	9.47E-01	8.35E+07(1.2%)	8.97E-01	8.05E+07	9.78E-01	8.73E+07
		1 - 1	60336	1657.379	5.67E-01	8.32E+07(1.2%)	5.37E-01	8.01E+07	5.84E-01	8.67E+07
		0 - 1	60317	1657.907	7.57E-01	3.33E+08(1.2%)	7.17E-01	3.20E+08	7.80E-01	3.47E+08
		1 - 0	60352	1656.928	7.57E-01	1.11E+08(1.2%)	7.17E-01	1.07E+08	7.81E-01	1.16E+08
		1 - 2	61938	1614.507	1.80E-04	2.86E+04(1.6%)	2.72E-04	4.40E+04	1.85E-04	2.97E+04
		1 - 1	61965	1613.803	1.65E-04	2.61E+04(1.0%)	1.62E-04	2.62E+04	1.74E-04	2.81E+04
		1 - 0	61981	1613.376	2.21E-04	3.51E+04(1.1%)	2.34E-04	3.79E+04	2.26E-04	3.65E+04
$2s2p^3 - 2s^2 2p^2$	$3^{\circ}\text{D}^{\circ} - 3^{\circ}\text{P}$	3 - 2	64043	1561.437	1.53E+00	1.22E+08(2.3%)	1.42E+00	1.14E+08	1.54E+00	1.19E+08
		2 - 2	64046	1561.366	2.72E-01	3.03E+07(2.1%)	2.52E-01	2.84E+07	2.75E-01	2.96E+07
		1 - 2	64047	1561.339	1.81E-02	3.35E+06(2.0%)	1.67E-02	3.14E+06	1.83E-02	3.28E+06
		2 - 1	64073	1560.708	8.22E-01	9.14E+07(2.2%)	7.60E-01	8.59E+07	8.28E-01	8.91E+07
		1 - 1	64074	1560.681	2.73E-01	5.06E+07(2.1%)	2.53E-01	4.76E+07	2.76E-01	4.94E+07
		1 - 0	64090	1560.282	3.65E-01	6.78E+07(2.1%)	3.38E-01	6.37E+07	3.68E-01	6.61E+07
		2 - 2	75212	1329.562	7.98E-01	1.42E+08(3.1%)	7.44E-01	1.35E+08	9.54E-01	1.66E+08
		1 - 2	75210	1329.600	2.69E-01	7.95E+07(3.1%)	2.51E-01	7.57E+07	3.20E-01	9.28E+07
		2 - 1	75239	1329.085	2.58E-01	4.58E+07(3.1%)	2.40E-01	4.34E+07	3.12E-01	5.44E+07
$2s^2 2p3d - 2s^2 2p^2$	$1^{\circ}\text{D}^{\circ} - 3^{\circ}\text{P}$	1 - 1	75237	1329.123	1.64E-01	4.85E+07(3.1%)	1.53E-01	4.63E+07	1.93E-01	5.60E+07
		0 - 1	75238	1329.100	2.17E-01	1.93E+08(3.1%)	2.04E-01	1.85E+08	2.57E-01	2.24E+08
		1 - 0	75254	1328.833	2.13E-01	6.30E+07(3.1%)	1.99E-01	6.00E+07	2.54E-01	7.37E+07
		2 - 2	77636	1288.055	4.63E-04	8.69E+04(1.4%)	4.27E-04	8.10E+04	3.51E-04	6.68E+04
		2 - 1	77663	1287.608	8.40E-04	1.58E+05(1.2%)	7.68E-04	1.46E+05	7.84E-04	1.49E+05
		2 - 2	78104	1280.333	3.23E-01	6.17E+07(0.7%)	3.21E-01	6.21E+07	3.30E-01	6.40E+07
		1 - 2	78073	1280.847	1.13E-01	3.59E+07(0.5%)	1.10E-01	3.55E+07	1.13E-01	3.63E+07
		2 - 1	78131	1279.890	1.96E-01	3.76E+07(0.5%)	1.81E-01	3.50E+07	1.77E-01	3.44E+07
		1 - 1	78100	1280.404	5.55E-02	1.77E+07(0.6%)	5.57E-02	1.79E+07	5.83E-02	1.88E+07
$2s^2 2p3d - 2s^2 2p^2$	$3^{\circ}\text{D}^{\circ} - 3^{\circ}\text{P}$	0 - 1	78088	1280.597	9.23E-02	8.82E+07(0.5%)	8.91E-02	8.61E+07	9.14E-02	8.84E+07
		1 - 0	78116	1280.135	1.16E-01	3.71E+07(0.5%)	1.11E-01	3.57E+07	1.10E-01	3.56E+07
		3 - 2	78274	1277.550	1.68E+00	2.31E+08(0.2%)	1.61E+00	2.23E+08	1.64E+00	2.28E+08
		2 - 2	78264	1277.723	3.44E-01	6.61E+07(0.1%)	3.22E-01	6.26E+07	3.24E-01	6.32E+07
		1 - 2	78250	1277.954	1.47E-02	4.70E+06(<0.05%)	1.72E-02	5.58E+06	1.84E-02	5.95E+06
		2 - 1	78291	1277.282	8.75E-01	1.68E+08(0.2%)	8.42E-01	1.64E+08	8.73E-01	1.70E+08
		1 - 1	78277	1277.513	2.43E-01	7.80E+07(0.1%)	2.66E-01	8.61E+07	2.85E-01	9.26E+07
		1 - 0	78293	1277.245	3.42E-01	1.10E+08(0.2%)	3.59E-01	1.17E+08	3.88E-01	1.26E+08
		1 - 2	78296	1277.190	1.14E-02	3.64E+06(0.4%)	6.78E-03	2.20E+06	5.59E-03	1.82E+06
$2s^2 2p4s - 2s^2 2p^2$	$1^{\circ}\text{P}^{\circ} - 3^{\circ}\text{P}$	1 - 1	78323	1276.750	7.84E-02	2.52E+07(0.2%)	3.90E-02	1.27E+07	2.89E-02	9.41E+06
		1 - 0	78340	1276.482	5.97E-02	1.92E+07(0.1%)	2.48E-02	8.05E+06	1.55E-02	5.05E+06
		3 - 2	78486	1274.109	1.00E-02	1.39E+06(0.1%)	1.18E-02	1.65E+06	8.60E-03	1.21E+06
$2s^2 2p3d - 2s^2 2p^2$	$1^{\circ}\text{P}^{\circ} - 3^{\circ}\text{P}$	1 - 2	78687	1270.844	1.77E-06	5.75E+02(0.4%)	3.03E-07	9.97E+01	1.28E-05	4.23E+03
		1 - 1	78714	1270.408	6.02E-04	1.96E+05(0.3%)	5.66E-04	1.87E+05	6.50E-04	2.15E+05
		1 - 0	78731	1270.143	1.65E-03	5.39E+05(0.1%)	1.61E-03	5.32E+05	1.38E-03	4.55E+05
$2s^2 2p3d - 2s^2 2p^2$	$3^{\circ}\text{P}^{\circ} - 3^{\circ}\text{P}$	2 - 2	79267	1261.552	8.17E-01	1.66E+08(2.1%)	8.13E-01	1.67E+08	6.65E-01	1.35E+08

Table A7. Continued.

Transition array	Mult.	$J_u - J_l$	ΔE (cm ⁻¹)	λ (Å)	MCDHF/RCI		Spline FCS ^(a)		MCHF-BP ^(b)	
					S (a.u. of $a_0^2 e^2$)	A (s ⁻¹)	S (a.u. of $a_0^2 e^2$)	A (s ⁻¹)	S (a.u. of $a_0^2 e^2$)	A (s ⁻¹)
$2s^2 2p3d - 2s^2 2p^2$	$3F^o - 1D$	1 - 2	79275	1261.425	2.74E-01	9.26E+07(2.1%)	2.72E-01	9.31E+07	2.23E-01	7.55E+07
		2 - 1	79294	1261.122	2.54E-01	5.15E+07(2.1%)	2.52E-01	5.19E+07	1.98E-01	4.02E+07
		1 - 1	79302	1260.996	1.69E-01	5.72E+07(2.1%)	1.68E-01	5.75E+07	1.39E-01	4.70E+07
		0 - 1	79306	1260.926	2.20E-01	2.24E+08(2.1%)	2.18E-01	2.24E+08	1.79E-01	1.82E+08
		1 - 0	79318	1260.735	2.12E-01	7.19E+07(2.1%)	2.11E-01	7.23E+07	1.69E-01	5.73E+07
	$3P^o - 1D$	2 - 2	68006	1470.449	4.71E-04	5.91E+04(1.4%)			4.22E-04	5.36E+04
		3 - 2	68022	1470.094	1.52E-02	1.36E+06(0.2%)			1.55E-02	1.41E+06
		1 - 2	50160	1993.620	1.04E-03	8.67E+04(1.4%)			9.65E-04	8.18E+04
		2 - 2	50200	1992.012	1.97E-05	9.90E+02(3.2%)			1.50E-05	7.66E+02
		1 - 2	51789	1930.905	3.59E+00	3.30E+08(1.5%)			3.62E+00	3.37E+08
$2s^2 2p3s - 2s^2 2p^2$	$3D^o - 1D$	3 - 2	53894	1855.483	9.91E-06	4.71E+02(24.2%)			6.60E-06	3.01E+02
		1 - 2	65061	1537.011	8.58E-06	1.65E+03(1.7%)			8.59E-08	1.60E+01
		2 - 2	65063	1536.960	2.51E-05	2.89E+03(6.9%)			7.15E-06	8.02E+02
		2 - 2	67487	1481.763	3.03E-01	3.72E+07(1.2%)			2.77E-01	3.45E+07
		1 - 2	67924	1472.231	4.55E-03	9.48E+05(1.6%)			3.68E-03	7.77E+05
	$3D^o - 1D$	2 - 2	67955	1471.552	2.02E-04	2.53E+04(1.0%)			1.77E-04	2.25E+04
		3 - 2	68125	1467.877	7.46E-03	6.72E+05(0.2%)			5.35E-03	4.88E+05
		2 - 2	68114	1468.106	5.36E-05	6.76E+03(2.9%)			7.36E-05	9.40E+03
		1 - 2	68100	1468.410	4.59E-02	9.64E+06(2.2%)			1.13E-02	2.40E+06
		1 - 2	68147	1467.402	2.36E-01	4.97E+07(2.0%)			2.57E-01	5.48E+07
$2s^2 2p3d - 2s^2 2p^2$	$1P^o - 1D$	3 - 2	68336	1463.336	1.99E+00	1.81E+08(0.3%)			1.94E+00	1.78E+08
		1 - 2	68538	1459.031	2.18E-01	4.66E+07(0.1%)			2.51E-01	5.44E+07
	$3P^o - 1D$	2 - 2	69118	1446.797	1.83E-05	2.46E+03(5.2%)			3.09E-05	4.13E+03
		1 - 2	69126	1446.630	4.50E-06	1.01E+03(5.4%)			2.65E-06	5.92E+02
		1 - 0	38704	2583.670	1.61E-04	6.13E+03(5.2%)			1.48E-04	5.72E+03
$2s^2 2p3s - 2s^2 2p^2$	$1P^o - 1S$	1 - 0	40333	2479.310	6.69E-01	2.89E+07(3.7%)			6.31E-01	2.76E+07
		3 - 2	53605	1865.464	6.83E-06	7.36E+02(23.2%)			2.71E-06	2.83E+02
		3 - 2	56468	1770.891	9.52E-05	1.13E+04(6.6%)			8.80E-05	1.06E+04
		3 - 2	56645	1765.366	1.32E-02	1.59E+06(2.9%)			6.33E-03	7.72E+05
		1 - 0	56692	1763.909	1.72E-02	2.07E+06(5.0%)			1.99E-02	2.43E+06
	$3P^o - 1S$	1 - 0	57083	1751.827	7.32E-01	9.00E+07(<0.05%)			6.67E-01	8.33E+07
		1 - 0	57670	1733.980	4.99E-05	6.48E+03(8.1%)			1.18E-04	1.53E+04
		2 - 2	83454	1198.262	3.73E-04	8.70E+04(0.8%)	2.87E-04	6.75E+04		
		2 - 1	83481	1197.875	1.03E-03	2.39E+05(0.8%)	8.64E-04	2.04E+05		
		2 - 2	83747	1194.063	1.18E-01	2.78E+07(0.9%)	1.25E-01	2.98E+07		
$2s^2 2p3d - 2s^2 2p^2$	$3P^o - 3P$	1 - 2	83704	1194.686	4.34E-02	1.70E+07(0.8%)	4.47E-02	1.77E+07		
		2 - 1	83774	1193.678	1.17E-01	2.75E+07(0.6%)	1.07E-01	2.54E+07		
		1 - 1	83731	1194.301	1.95E-02	7.67E+06(0.9%)	2.10E-02	8.34E+06		
		0 - 1	83723	1194.405	3.64E-02	4.29E+07(0.7%)	3.70E-02	4.40E+07		
		1 - 0	83747	1194.066	4.98E-02	1.95E+07(0.7%)	4.90E-02	1.94E+07		
	$3D^o - 3P$	3 - 2	83805	1193.240	6.80E-01	1.15E+08(0.1%)	6.52E-01	1.11E+08		
		2 - 2	83794	1193.393	1.57E-01	3.70E+07(0.1%)	1.45E-01	3.46E+07		
		1 - 2	83776	1193.649	5.60E-03	2.20E+06(0.1%)	5.67E-03	2.25E+06		
		2 - 1	83821	1193.009	3.37E-01	7.95E+07(<0.05%)	3.31E-01	7.90E+07		
		1 - 1	83803	1193.264	1.10E-01	4.31E+07(<0.05%)	1.08E-01	4.29E+07		
$2s^2 2p3s - 2s^2 2p^2$	$1P^o - 3P$	1 - 0	83820	1193.030	1.65E-01	6.50E+07(0.1%)	1.61E-01	6.39E+07		
		1 - 2	83833	1192.835	6.48E-03	2.55E+06(0.5%)	5.50E-03	2.19E+06		
		1 - 1	83860	1192.451	2.38E-02	9.38E+06(0.3%)	1.91E-02	7.61E+06		
		1 - 0	83877	1192.218	7.36E-03	2.90E+06(0.3%)	5.39E-03	2.15E+06		
		3 - 2	83903	1191.841	1.54E-02	2.61E+06(0.1%)	1.70E-02	2.90E+06		
	$1P^o - 3P$	1 - 2	83988	1190.636	3.47E-05	1.37E+04(0.3%)	3.15E-05	1.26E+04		
		1 - 1	84015	1190.253	1.25E-03	4.93E+05(0.1%)	1.20E-03	4.79E+05		
		1 - 0	84032	1190.021	2.39E-03	9.48E+05(<0.05%)	2.26E-03	9.05E+05		
		2 - 2	84059	1189.631	2.38E-01	5.68E+07(1.0%)	2.19E-01	5.28E+07		
		1 - 2	84072	1189.447	8.04E-02	3.20E+07(1.0%)	7.37E-02	2.96E+07		
$2s^2 2p3d - 2s^2 2p^2$	$3P^o - 3P$	2 - 1	84086	1189.249	5.07E-02	1.21E+07(1.1%)	4.53E-02	1.09E+07		
		1 - 1	84099	1189.065	5.43E-02	2.16E+07(1.0%)	5.01E-02	2.02E+07		
		0 - 1	84104	1188.993	6.52E-02	7.79E+07(1.0%)	5.96E-02	7.19E+07		
		1 - 0	84116	1188.833	5.35E-02	2.13E+07(1.1%)	4.86E-02	1.96E+07		
		2 - 2	86141	1160.876	6.52E-04	1.67E+05(<0.05%)	4.58E-04	1.19E+05		
	$3D^o - 3P$	2 - 1	86168	1160.513	1.50E-03	3.86E+05(0.8%)	1.26E-03	3.27E+05		
		2 - 2	86325	1158.400	2.62E-02	6.76E+06(0.1%)	3.15E-02	8.19E+06		
		1 - 2	86288	1158.907	1.78E-02	7.62E+06(0.2%)	1.93E-02	8.36E+06		
		2 - 1	86352	1158.038	1.27E-01	3.29E+07(0.2%)	1.19E-01	3.10E+07		
		1 - 1	86315	1158.544	6.63E-03	2.85E+06(0.4%)	7.73E-03	3.36E+06		
$2s^2 2p3d - 2s^2 2p^2$	$3P^o - 3P$	0 - 1	86305	1158.674	1.57E-02	2.02E+07(0.3%)	1.68E-02	2.19E+07		
		1 - 0	86331	1158.324	2.44E-02	1.05E+07(0.1%)	2.50E-02	1.09E+07		
		3 - 2	86354	1158.018	3.20E-01	5.90E+07(0.3%)	2.99E-01	5.56E+07		
		2 - 2	86346	1158.131	1.05E-01	2.71E+07(<0.05%)	9.90E-02	2.58E+07		
		1 - 2	86319	1158.492	1.37E-03	5.88E+05(0.2%)	1.45E-03	6.29E+05		
	$3D^o - 3P$	2 - 1	86373	1157.769	1.03E-01	2.65E+07(0.4%)	1.00E-01	2.62E+07		
		1 - 1	86346	1158.130	4.69E-02	2.02E+07(0.2%)	4.55E-02	1.98E+07		
		1 - 0	86362	1157.909	8.57E-02	3.69E+07(0.3%)	8.08E-02	3.51E+07		

^(a) Zatsarinny & Fischer (2002); ^(b) Fischer (2006).

Table A8. Comparison of line strengths (S) and transition rates (A) with other theoretical results for C II. The present values from the MCDHF/RCI calculations are given in the Babushkin(length) gauge. The wavenumber ΔE and wavelength λ values are taken from the NIST database. The estimated uncertainties dT of the transition rates are given as percentages in parentheses.

Transition array	Mult.	$J_u - J_l$	ΔE (cm ⁻¹)	λ (Å)	MCDHF/RCI		MCHF-BP ^(a)		CIV3 ^(b)
					S (a.u. of $a_0^2 e^2$)	A (s ⁻¹)	S (a.u. of $a_0^2 e^2$)	A (s ⁻¹)	A (s ⁻¹)
2s2p ² – 2s ² 2p	2D – 2P ^o	5/2 – 3/2	74866	1335.708	2.03E+00	2.89E+08(0.2%)	2.03E+00	2.90E+08	2.89E+08
		3/2 – 3/2	74869	1335.663	2.24E-01	4.79E+07(<0.05%)	2.24E-01	4.80E+07	4.79E+07
		3/2 – 1/2	74932	1334.532	1.13E+00	2.42E+08(0.1%)	1.13E+00	2.43E+08	2.42E+08
2s2p ² – 2s ² 2p	2S – 2P ^o	1/2 – 3/2	96430	1037.018	1.62E+00	1.48E+09(0.7%)	1.61E+00	1.47E+09	1.47E+09
		1/2 – 1/2	96493	1036.337	8.18E-01	7.48E+08(0.6%)	8.11E-01	7.43E+08	7.46E+08
2s2p ² – 2s ² 2p	2P – 2P ^o	1/2 – 3/2	110560	904.480	9.96E-01	1.37E+09(0.3%)	9.96E-01	1.37E+09	1.36E+09
		3/2 – 3/2	110602	904.142	4.95E+00	3.41E+09(0.4%)	4.94E+00	3.41E+09	3.38E+09
		1/2 – 1/2	110624	903.962	1.97E+00	2.72E+09(0.4%)	1.97E+00	2.72E+09	2.69E+09
2s ² 3s – 2s ² 2p	2S – 2P ^o	3/2 – 1/2	110665	903.623	9.88E-01	6.82E+08(0.4%)	9.87E-01	6.82E+08	6.76E+08
		1/2 – 3/2	116474	858.559	1.81E-01	2.89E+08(0.6%)	1.83E-01	2.93E+08	2.83E+08
		1/2 – 1/2	116537	858.092	9.19E-02	1.47E+08(0.6%)	9.28E-02	1.49E+08	1.44E+08
2s ² 3d – 2s ² 2p	2D – 2P ^o	3/2 – 3/2	145485	687.352	3.03E-01	4.71E+08(0.2%)	3.02E-01	4.70E+08	4.60E+08
		5/2 – 3/2	145487	687.345	2.72E+00	2.82E+09(0.2%)	2.71E+00	2.82E+09	2.76E+09
		3/2 – 1/2	145549	687.053	1.51E+00	2.35E+09(0.2%)	1.51E+00	2.35E+09	2.30E+09
2s ² 3p – 2s2p ²	2P ^o – 4P	3/2 – 5/2	88681	1127.626	6.13E-07	2.16E+02(2.0%)	5.04E-07	1.79E+02	1.80E+02
		3/2 – 5/2	98973	1010.371	3.45E+00	1.70E+09(0.4%)	3.44E+00	1.70E+09	1.71E+09
2p ³ – 2s2p ²	4S ^o – 4P	3/2 – 3/2	99001	1010.083	2.30E+00	1.13E+09(0.4%)	2.30E+00	1.13E+09	1.14E+09
		3/2 – 1/2	99023	1009.858	1.15E+00	5.67E+08(0.4%)	1.15E+00	5.67E+08	5.69E+08
		5/2 – 5/2	107407	931.030	4.41E-06	1.86E+03(21.1%)	3.52E-06	1.48E+03	1.50E+03
2p ³ – 2s2p ²	2D ^o – 4P	3/2 – 3/2	107441	930.740	1.04E-06	6.59E+02(22.2%)	8.44E-07	5.33E+02	5.39E+02
		3/2 – 5/2	123937	806.861	6.36E-01	6.13E+08(0.4%)	3.93E-01	3.79E+08	
		1/2 – 3/2	123941	806.830	5.88E-01	1.13E+09(0.4%)	3.64E-01	7.02E+08	
2s ² 3s – 2s2p ²	4P ^o – 4P	1/2 – 1/2	123963	806.687	1.18E-01	2.27E+08(0.4%)	7.27E-02	1.40E+08	
		3/2 – 3/2	123965	806.677	1.88E-01	1.81E+08(0.4%)	1.16E-01	1.12E+08	
		5/2 – 5/2	123982	806.568	1.48E+00	9.53E+08(0.4%)	9.16E-01	5.90E+08	
2p ³ – 2s2p ²	2P ^o – 4P	3/2 – 1/2	123987	806.533	5.88E-01	5.67E+08(0.4%)	3.63E-01	3.51E+08	
		5/2 – 3/2	124010	806.384	6.35E-01	4.09E+08(0.4%)	3.92E-01	2.53E+08	
		3/2 – 5/2	125924	794.125	2.69E-05	2.72E+04(3.2%)	7.77E-06	7.83E+03	1.72E+02
2s ² 3p – 2s2p ²	2P ^o – 2D	1/2 – 3/2	125953	793.947	4.39E-06	8.88E+03(0.3%)	3.80E-06	7.65E+03	1.88E+02
		3/2 – 3/2	125953	793.947	1.60E-06	1.62E+03(8.6%)	8.35E-06	8.42E+03	1.57E+03
		1/2 – 1/2	125975	793.808	1.51E-06	3.06E+03(10.2%)	1.73E-06	3.50E+03	2.04E+01
2s ² 3p – 2s2p ²	2P ^o – 2D	3/2 – 1/2	125975	793.808	1.44E-05	1.46E+04(2.7%)	2.48E-05	2.50E+04	6.67E+02
		1/2 – 3/2	56791	1760.819	2.23E-01	4.09E+07(1.6%)	2.20E-01	4.08E+07	4.37E+07
		3/2 – 3/2	56802	1760.473	4.45E-02	4.09E+06(1.6%)	4.40E-02	4.07E+06	4.37E+06
2p ³ – 2s2p ²	2D ^o – 2D	3/2 – 5/2	56805	1760.395	4.01E-01	3.68E+07(1.6%)	3.96E-01	3.67E+07	3.94E+07
		5/2 – 3/2	75528	1323.995	2.27E-01	3.33E+07(0.2%)	2.25E-01	3.28E+07	3.50E+07
		5/2 – 5/2	75531	1323.951	3.16E+00	4.63E+08(0.1%)	3.13E+00	4.56E+08	4.88E+08
2s ² 3s – 2s2p ²	4P ^o – 2D	3/2 – 3/2	75534	1323.906	2.03E+00	4.45E+08(0.1%)	2.01E+00	4.39E+08	4.69E+08
		3/2 – 5/2	75536	1323.862	2.30E-01	5.05E+07(<0.05%)	2.27E-01	4.96E+07	5.31E+07
		1/2 – 3/2	92034	1086.549	1.55E-05	1.21E+04(1.0%)	2.45E-05	1.93E+04	
2p ³ – 2s2p ²	2P ^o – 2D	3/2 – 3/2	92058	1086.270	1.50E-05	5.88E+03(1.4%)	2.13E-05	8.39E+03	
		3/2 – 5/2	92060	1086.241	9.46E-05	3.71E+04(0.9%)	1.50E-04	5.93E+04	
		5/2 – 5/2	92105	1085.710	3.20E-06	8.38E+02(3.6%)	2.45E-06	6.45E+02	
2s ² 3p – 2s2p ²	2P ^o – 2S	1/2 – 3/2	94045	1063.313	1.97E+00	1.65E+09(0.9%)	1.73E+00	1.45E+09	1.63E+09
		3/2 – 3/2	94045	1063.313	3.97E-01	1.66E+08(0.9%)	3.44E-01	1.44E+08	1.64E+08
		3/2 – 5/2	94048	1063.284	3.55E+00	1.49E+09(0.8%)	3.11E+00	1.30E+09	1.46E+09
2p ³ – 2s2p ²	2D ^o – 2S	1/2 – 1/2	35230	2838.439	7.05E-01	3.06E+07(0.1%)	7.44E-01	3.27E+07	3.32E+07
		3/2 – 1/2	35241	2837.541	1.41E+00	3.06E+07(0.1%)	1.49E+00	3.28E+07	3.32E+07
		3/2 – 1/2	53972	1852.780	1.78E-05	1.43E+03(1.8%)	1.55E-05	1.23E+03	1.46E+03
2p ³ – 2s2p ²	2P ^o – 2S	1/2 – 1/2	72484	1379.603	1.55E-05	5.92E+03(59.0%)	1.02E-01	3.87E+07	2.50E+04
		3/2 – 1/2	72484	1379.603	1.78E-04	3.39E+04(31.6%)	2.13E-01	4.05E+07	6.94E+04
		1/2 – 3/2	21058	4748.606	2.62E-03	2.37E+04(5.9%)	2.46E-03	2.31E+04	2.52E+04
2s ² 3p – 2s2p ²	2P ^o – 2P	3/2 – 3/2	21069	4746.093	1.35E-02	6.12E+04(5.6%)	1.26E-02	5.92E+04	6.53E+04
		1/2 – 1/2	21100	4739.292	6.33E-03	5.76E+04(5.2%)	5.75E-03	5.42E+04	6.12E+04
		3/2 – 1/2	21111	4736.789	1.87E-03	8.54E+03(6.5%)	1.90E-03	8.96E+03	9.23E+03
2p ³ – 2s2p ²	2D ^o – 2P	5/2 – 3/2	39796	2512.814	2.68E+00	5.73E+07(2.7%)	2.64E+00	5.62E+07	6.20E+07
		3/2 – 3/2	39801	2512.491	2.95E-01	9.45E+06(2.6%)	2.90E-01	9.28E+06	1.02E+07
		3/2 – 1/2	39842	2509.881	1.49E+00	4.81E+07(2.6%)	1.47E+00	4.72E+07	5.21E+07
2s ² 3s – 2s2p ²	4P ^o – 2P	1/2 – 3/2	56301	1776.149	4.38E-06	7.80E+02(0.4%)	9.53E-06	1.71E+03	
		3/2 – 3/2	56325	1775.405	5.90E-05	5.25E+03(0.4%)	1.53E-04	1.37E+04	
		1/2 – 1/2	56342	1774.845	4.89E-06	8.72E+02(0.5%)	1.55E-05	2.78E+03	
2p ³ – 2s2p ²	2P ^o – 2P	3/2 – 1/2	56366	1774.102	1.29E-05	1.15E+03(0.3%)	3.19E-05	2.88E+03	
		1/2 – 3/2	58312	1714.890	5.79E-01	1.14E+08(0.3%)	8.67E-01	1.71E+08	1.12E+08
		3/2 – 3/2	58312	1714.890	2.91E+00	2.88E+08(0.3%)	4.36E+00	4.31E+08	2.83E+08
2s ² 3p – 2s ² 3s	2P ^o – 2S	1/2 – 1/2	58354	1713.674	1.16E+00	2.30E+08(0.3%)	1.74E+00	3.44E+08	2.26E+08
		3/2 – 1/2	58354	1713.674	5.79E-01	5.74E+07(0.3%)	8.70E-01	8.62E+07	5.63E+07
		1/2 – 1/2	15186	6584.700	1.03E+01	3.64E+07(0.2%)	1.03E+01	3.78E+07	3.70E+07
2p ³ – 2s ² 3s	2P ^o – 2S	3/2 – 1/2	15197	6579.869	2.06E+01	3.65E+07(0.3%)	2.06E+01	3.79E+07	3.71E+07
		1/2 – 1/2	52440	1906.916	2.19E-02	3.19E+06(0.1%)	6.60E-02	9.58E+06	3.35E+06
		3/2 – 1/2	52440	1906.916	4.31E-02	3.15E+06(0.1%)	1.30E-01	9.45E+06	3.32E+06
2s ² 3d – 2s ² 3p	2D – 2P ^o	3/2 – 3/2	13813	7239.164	5.20E+00	6.94E+06(0.6%)	5.21E+00	6.73E+06	7.09E+06
		5/2 – 3/2	13815	7238.415	4.68E+01	4.17E+07(0.6%)	4.69E+01	4.04E+07	4.25E+07
		3/2 – 1/2	13824	7233.325	2.60E+01	3.48E+07(0.6%)	2.60E+01	3.37E+07	3.55E+07
2p ³ – 2s ² 3d	2P ^o – 2D	1/2 – 3/2	23429	4268.202	9.99E-05	1.30E+03(27.0%)	3.11E-01	3.99E+06	4.08E+04

Table A8. Continued.

Transition array	Mult.	$J_u - J_l$	ΔE (cm ⁻¹)	λ (Å)	MCDHF/RCI		MCHF-BP ^(a)		CIV3 ^(b) A (s ⁻¹)
					S (a.u. of $a_0^2 e^2$)	A (s ⁻¹)	S (a.u. of $a_0^2 e^2$)	A (s ⁻¹)	
		3/2 - 5/2	23427	4268.462	1.15E-04	7.49E+02(32.7%)	5.57E-01	3.58E+06	3.33E+04

^(a)Tachiev & Fischer (2000); ^(b)Corr  g   & Hibbert (2004).**Table A9.** Comparison of line strengths (S) and transition rates (A) with other theoretical results for C III. The present values from the MCDHF/RCI calculations are given in the Babushkin(length) gauge. The wavenumber ΔE and wavelength λ values are taken from the NIST database. The estimated uncertainties dT of the transition rates are given as percentages in parentheses.

Transition array	Mult.	$J_u - J_l$	ΔE (cm ⁻¹)	λ (Å)	MCDHF/RCI		MCHF-BP ^(a)		GRASP ^(b)	
					S (a.u. of $a_0^2 e^2$)	A (s ⁻¹)	S (a.u. of $a_0^2 e^2$)	A (s ⁻¹)	S (a.u. of $a_0^2 e^2$)	A (s ⁻¹)
2s2p – 2s ²	1p ^o – 1s	1 - 0	102352	977.020	2.44E+00	1.77E+09(0.1%)	2.44E+00	1.77E+09	2.38E+00	2.15E+09
2s3p – 2s ²	1p ^o – 1s	1 - 0	258931	386.203	3.06E-01	3.59E+09(<0.05%)	3.06E-01	3.59E+09	2.70E-01	3.16E+09
2s3p – 2s ²	3p ^o – 1s	1 - 0	259711	385.043	4.29E-05	5.08E+05(0.5%)	4.37E-05	5.18E+05	1.17E-02	1.36E+08
2p ² – 2s2p	3p – 3p ^o	1 - 2	85007	1176.370	1.32E+00	5.48E+08(<0.05%)	1.32E+00	5.50E+08	1.33E+00	5.95E+08
		0 - 1	85034	1175.987	1.05E+00	1.32E+09(0.1%)	1.05E+00	1.32E+09	1.07E+00	1.43E+09
		2 - 2	85054	1175.711	3.95E+00	9.89E+08(0.1%)	3.95E+00	9.91E+08	4.00E+00	1.07E+09
		1 - 1	85063	1175.590	7.90E-01	3.30E+08(0.1%)	7.89E-01	3.31E+08	8.00E-01	3.58E+08
		1 - 0	85087	1175.263	1.05E+00	4.40E+08(0.1%)	1.05E+00	4.41E+08	1.07E+00	4.78E+08
		2 - 1	85111	1174.933	1.32E+00	3.30E+08(0.1%)	1.32E+00	3.31E+08	1.33E+00	3.59E+08
2p ² – 2s2p	1D – 3p ^o	2 - 2	93429	1070.331	9.42E-05	3.13E+04(5.3%)	9.51E-05	3.17E+04	3.74E-05	1.51E+04
		2 - 1	93485	1069.686	1.36E-05	4.52E+03(7.8%)	1.49E-05	4.97E+03	3.37E-06	1.37E+03
2p ² – 2s2p	1S – 3p ^o	0 - 1	130129	768.467	4.58E-07	2.06E+03(17.8%)	4.71E-07	2.12E+03	2.01E-07	1.14E+03
2s3s – 2s2p	3S – 3p ^o	1 - 2	185765	538.312	4.73E-01	2.05E+09(0.1%)	4.73E-01	2.05E+09	5.03E-01	2.11E+09
		1 - 1	185822	538.149	2.83E-01	1.23E+09(0.1%)	2.84E-01	1.23E+09	3.01E-01	1.27E+09
		1 - 0	185845	538.080	9.43E-02	4.09E+08(0.1%)	9.45E-02	4.10E+08	1.00E-01	4.22E+08
2s3s – 2s2p	1S – 3p ^o	0 - 1	194779	513.401	1.45E-08	2.17E+02(25.2%)	1.76E-08	2.64E+02	2.46E-08	3.60E+02
2s3d – 2s2p	3D – 3p ^o	1 - 2	217563	459.635	4.24E-02	2.95E+08(<0.05%)	4.24E-02	2.95E+08	4.24E-02	2.88E+08
		2 - 2	217564	459.633	6.36E-01	2.65E+09(<0.05%)	6.36E-01	2.66E+09	6.36E-01	2.60E+09
		3 - 2	217567	459.627	3.56E+00	1.06E+10(<0.05%)	3.56E+00	1.06E+10	3.56E+00	1.04E+10
		1 - 1	217620	459.516	6.36E-01	4.43E+09(<0.05%)	6.36E-01	4.43E+09	6.36E-01	4.33E+09
		2 - 1	217621	459.514	1.91E+00	7.96E+09(<0.05%)	1.91E+00	7.97E+09	1.91E+00	7.79E+09
		1 - 0	217643	459.466	8.47E-01	5.90E+09(<0.05%)	8.47E-01	5.91E+09	8.48E-01	5.77E+09
2s3d – 2s2p	1D – 3p ^o	2 - 1	224092	446.245	4.65E-07	2.12E+03(0.3%)	2.80E-07	1.28E+03	2.48E-07	1.14E+03
2p ² – 2s2p	3P – 1p ^o	0 - 1	35073	2851.142	2.69E-06	2.36E+02(37.5%)	2.99E-06	2.65E+02	1.85E-06	1.02E+02
		2 - 1	35149	2844.953	7.79E-05	1.37E+03(8.2%)	8.02E-05	1.43E+03	2.85E-05	3.15E+02
2p ² – 2s2p	1D – 1p ^o	2 - 1	43524	2297.578	4.11E+00	1.38E+08(0.5%)	4.11E+00	1.39E+08	4.18E+00	1.34E+08
2p ² – 2s2p	1S – 1p ^o	0 - 1	80167	1247.383	1.99E+00	2.10E+09(<0.05%)	1.99E+00	2.10E+09	2.24E+00	2.69E+09
2s3s – 2s2p	3S – 1p ^o	1 - 1	135860	736.047	4.69E-07	7.92E+02(5.0%)	5.42E-07	9.17E+02	3.76E-07	5.18E+02
2s3s – 2s2p	1S – 1p ^o	0 - 1	144818	690.521	1.40E-01	8.59E+08(0.1%)	1.39E-01	8.54E+08	1.77E-01	9.10E+08
2s3d – 2s2p	3D – 1p ^o	1 - 1	167658	596.449	5.91E-07	1.88E+03(6.5%)	7.50E-07	2.39E+03	4.14E-07	1.12E+03
		2 - 1	167659	596.446	9.30E-07	1.77E+03(6.2%)	4.89E-07	9.34E+02	3.79E-07	6.15E+02
2s3d – 2s2p	1D – 1p ^o	2 - 1	174130	574.281	2.93E+00	6.25E+09(<0.05%)	2.92E+00	6.25E+09	3.37E+00	6.40E+09
2s3p – 2p ²	1p ^o – 3p	1 - 2	121429	823.525	1.05E-05	1.27E+04(0.3%)	1.07E-05	1.29E+04	7.12E-06	7.96E+03
		1 - 1	121476	823.202	1.76E-07	2.12E+02(1.0%)	8.87E-08	1.07E+02	1.41E-05	1.58E+04
2s3p – 2p ²	3p ^o – 3p	1 - 2	122209	818.269	7.20E-04	8.84E+05(0.2%)	7.05E-04	8.65E+05	6.36E-04	7.10E+05
		2 - 2	122222	818.181	2.17E-03	1.60E+06(0.2%)	2.15E-03	1.58E+06	1.91E-03	1.28E+06
		0 - 1	122251	817.988	5.76E-04	2.13E+06(0.2%)	5.65E-04	2.08E+06	5.08E-04	1.70E+06
		1 - 1	122256	817.950	4.29E-04	5.27E+05(0.2%)	4.26E-04	5.23E+05	3.63E-04	4.06E+05
		2 - 1	122269	817.863	7.30E-04	5.39E+05(0.3%)	7.20E-04	5.31E+05	6.43E-04	4.31E+05
		1 - 0	122285	817.758	5.78E-04	7.12E+05(0.2%)	5.69E-04	7.00E+05	4.86E-04	5.44E+05
2s3p – 2p ²	1p ^o – 1D	1 - 2	113055	884.524	3.77E-01	3.66E+08(<0.05%)	3.69E-01	3.59E+08	7.16E-01	5.67E+08
2s3p – 2p ²	3p ^o – 1D	1 - 2	113835	878.464	6.05E-05	6.00E+04(0.1%)	6.32E-05	6.27E+04	3.07E-02	2.43E+07
2s3p – 2p ²	1p ^o – 1S	1 - 0	76411	1308.705	7.24E-02	2.16E+07(0.1%)	7.20E-02	2.15E+07	1.54E-01	2.79E+07
2s3p – 2p ²	3p ^o – 1S	1 - 0	77191	1295.482	1.04E-05	3.19E+03(0.2%)	1.05E-05	3.23E+03	6.65E-03	1.20E+06
2s3p – 2s3s	1p ^o – 3S	1 - 1	20718	4826.653	1.65E-03	9.96E+03(1.7%)	1.69E-03	1.02E+04	4.51E-01	3.08E+06
2s3p – 2s3s	3p ^o – 3S	0 - 1	21492	4652.775	3.57E+00	7.20E+07(<0.05%)	3.57E+00	7.19E+07	3.65E+00	7.44E+07
		1 - 1	21498	4651.548	1.07E+01	7.20E+07(<0.05%)	1.07E+01	7.20E+07	1.05E+01	7.14E+07
		2 - 1	21511	4648.720	1.78E+01	7.22E+07(<0.05%)	1.78E+01	7.21E+07	1.83E+01	7.46E+07
2s3p – 2s3s	1p ^o – 1S	1 - 0	11761	8502.657	9.25E+00	1.02E+07(<0.05%)	9.25E+00	1.02E+07	8.59E+00	1.02E+07
2s3p – 2s3s	3p ^o – 1S	1 - 0	12540	7973.871	1.42E-03	1.89E+03(2.6%)	1.45E-03	1.92E+03	3.69E-01	4.33E+05
2s3d – 2s3p	3D – 1p ^o	1 - 1	11079	9025.645	6.66E-04	6.10E+02(1.6%)	6.87E-04	6.35E+02	1.86E-01	1.44E+05
		2 - 1	11080	9024.749	2.12E-03	1.17E+03(1.4%)	2.23E-03	1.24E+03	5.55E-01	2.58E+05
2s3d – 2s3p	1D – 1p ^o	2 - 1	17551	5697.496	1.94E+01	4.26E+07(<0.05%)	1.94E+01	4.28E+07	1.88E+01	5.15E+07
2s3d – 2s3p	3D – 3p ^o	1 - 2	10286	9721.451	2.94E-01	2.16E+05(<0.05%)	2.94E-01	2.18E+05	3.00E-01	2.35E+05
		2 - 2	10287	9720.412	4.40E+00	1.95E+06(<0.05%)	4.41E+00	1.97E+06	4.51E+00	2.11E+06
		3 - 2	10290	9717.757	2.47E+01	7.79E+06(<0.05%)	2.47E+01	7.87E+06	2.52E+01	8.46E+06
		1 - 1	10299	9709.105	4.40E+00	3.25E+06(<0.05%)	4.41E+00	3.29E+06	4.32E+00	3.39E+06
		2 - 1	10300	9708.069	1.32E+01	5.86E+06(<0.05%)	1.32E+01	5.92E+06	1.30E+01	6.10E+06
		1 - 0	10305	9703.764	5.87E+00	4.35E+06(<0.05%)	5.88E+00	4.39E+06	6.01E+00	4.72E+06
2s3d – 2s3p	1D – 3p ^o	2 - 1	16771	5962.446	3.11E-03	5.97E+03(0.4%)	3.23E-03	6.24E+03	8.04E-01	2.22E+06

^(a)Tachiev & Fischer (1999); ^(b)Aggarwal & Keenan (2015).

Table A10. Comparison of line strengths (S) and transition rates (A) with other theoretical results for C IV. The present values from the MCDHF/RCI calculations are given in the Babushkin(length) gauge. The wavenumber ΔE and wavelength λ values are taken from the NIST database. The estimated uncertainties dT of the transition rates are given as percentages in parentheses.

Transition array	Mult.	$J_u - J_l$	ΔE (cm ⁻¹)	λ (Å)	MCDHF/RCI		MCHF-BP ^(a)	
					S (a.u. of $a_0^2 e^2$)	A (s ⁻¹)	S (a.u. of $a_0^2 e^2$)	A (s ⁻¹)
2p – 2s	² P ^o – ² S	1/2 - 1/2	64484	1550.772	9.68E-01	2.63E+08(<0.05%)	9.68E-01	2.63E+08
		3/2 - 1/2	64591	1548.187	1.94E+00	2.65E+08(<0.05%)	1.94E+00	2.65E+08
3p – 2s	² P ^o – ² S	1/2 - 1/2	320050	312.451	1.39E-01	4.63E+09(<0.05%)	1.40E-01	4.64E+09
		3/2 - 1/2	320081	312.420	2.78E-01	4.62E+09(<0.05%)	2.79E-01	4.63E+09
3s – 2p	² S – ² P ^o	1/2 - 3/2	238257	419.714	2.07E-01	2.84E+09(<0.05%)	2.07E-01	2.84E+09
		1/2 - 1/2	238365	419.525	1.03E-01	1.42E+09(<0.05%)	1.03E-01	1.42E+09
3d – 2p	² D – ² P ^o	3/2 - 3/2	260288	384.190	3.26E-01	2.91E+09(<0.05%)	3.26E-01	2.91E+09
		5/2 - 3/2	260298	384.174	2.94E+00	1.75E+10(<0.05%)	2.94E+00	1.75E+10
		3/2 - 1/2	260395	384.031	1.63E+00	1.46E+10(<0.05%)	1.63E+00	1.46E+10
4s – 2p	² S – ² P ^o	1/2 - 3/2	336756	296.951	2.74E-02	1.06E+09(<0.05%)	2.75E-02	1.06E+09
		1/2 - 1/2	336864	296.856	1.37E-02	5.30E+08(<0.05%)	1.38E-02	5.32E+08
3p – 3s	² P ^o – ² S	1/2 - 1/2	17201	5813.582	6.10E+00	3.15E+07(<0.05%)	6.11E+00	3.15E+07
		3/2 - 1/2	17232	5802.921	1.22E+01	3.17E+07(<0.05%)	1.22E+01	3.16E+07
3d – 3p	² D – ² P ^o	3/2 - 3/2	4798	20841.583	1.71E+00	9.54E+04(<0.05%)	1.71E+00	9.51E+04
		5/2 - 3/2	4808	20796.074	1.54E+01	5.76E+05(<0.05%)	1.54E+01	5.74E+05
		3/2 - 1/2	4829	20705.220	8.54E+00	4.87E+05(<0.05%)	8.54E+00	4.85E+05
4s – 3p	² S – ² P ^o	1/2 - 3/2	81266	1230.521	1.32E+00	7.16E+08(<0.05%)	1.31E+00	7.14E+08
		1/2 - 1/2	81298	1230.043	6.57E-01	3.58E+08(<0.05%)	6.57E-01	3.57E+08

^(a)Fischer et al. (1998).

This paper has been typeset from a TeX/L^AT_EX file prepared by the author.